Space Sci Rev (2009) 145: 55–106
DOI 10.1007/s11214-008-9438-9

Plasmaspheric Density Structures and Dynamics: Properties Observed by the CLUSTER and IMAGE Missions

Fabien Darrouzet · Dennis L. Gallagher · Nicolas André · Donald L. Carpenter · Iannis Dandouras · Pierrette M.E. Décréau · Johan De Keyser · Richard E. Denton · John C. Foster · Jerry Goldstein · Mark B. Moldwin · Bodo W. Reinisch · Bill R. Sandel · Jiannan Tu

Received: 9 July 2008 / Accepted: 4 August 2008 / Published online: 12 November 2008

Abstract Plasmaspheric density structures have been studied since the discovery of the plasmasphere in the late 1950s. But the advent of the CLUSTER and IMAGE missions in 2000 has added substantially to our knowledge of density structures, thanks to the new

F. Darrouzet (✉) · J. De Keyser
Belgian Institute for Space Aeronomy (IASB-BIRA), 3 Avenue Circulaire, 1180 Brussels, Belgium
e-mail: Fabien.Darrouzet@oma.be

J. De Keyser
e-mail: Johan.DeKeyser@oma.be

D.L. Gallagher
Marshall Space Flight Center (MSFC), NASA, Huntsville, AL, USA
e-mail: dennis.l.gallagher@nasa.gov

N. André
Research and Scientific Support Department (RSSD), ESA, Noordwijk, The Netherlands
e-mail: nandre@rssd.esa.int

D.L. Carpenter
Space, Telecommunications and Radioscience Laboratory (STAR), Stanford University, Stanford, CA, USA
e-mail: dlc@nova.stanford.edu

I. Dandouras
Centre d'Etude Spatiale des Rayonnements (CESR), CNRS/Université de Toulouse, Toulouse, France
e-mail: Iannis.Dandouras@cesr.fr

P.M.E. Décréau
Laboratoire de Physique et Chimie de l'Environnement (LPCE), CNRS/Université d'Orléans, Orléans, France
e-mail: Pierrette.Decreau@cnrs-orleans.fr

R.E. Denton
Physics and Astronomy Department, Dartmouth College, Hanover, NH, USA
e-mail: richard.e.denton@dartmouth.edu

capabilities of those missions: global imaging with IMAGE and four-point in situ measurements with CLUSTER. The study of plasma sources and losses has given new results on refilling rates and erosion processes. Two-dimensional density images of the plasmasphere have been obtained. The spatial gradient of plasmaspheric density has been computed. The ratios between H^+, He^+ and O^+ have been deduced from different ion measurements. Plasmaspheric plumes have been studied in detail with new tools, which provide information on their morphology, dynamics and occurrence. Density structures at smaller scales have been revealed with those missions, structures that could not be clearly distinguished before the global images from IMAGE and the four-point measurements by CLUSTER became available. New terms have been given to these structures, like "shoulders", "channels", "fingers" and "crenulations". This paper reviews the most relevant new results about the plasmaspheric plasma obtained since the start of the CLUSTER and IMAGE missions.

Keywords Plasmasphere · CLUSTER · IMAGE · Plasma Structures

1 Introduction

From the discovery of the plasmasphere and its outer boundary, the plasmapause, in the 1950s (Storey 1953; Gringauz et al. 1960; Carpenter 1963) to the start of the CLUSTER (Escoubet et al. 1997) and IMAGE (Imager for Magnetopause-to-Aurora Global Exploration) (Burch 2000) missions in 2000, many studies of plasmaspheric density structures have been done with in situ measurements and ground-based observations (for more details, see the monograph by Lemaire and Gringauz 1998). However, those two missions completely changed the view of this region, thanks to their new capabilities: multipoint in situ measurements by CLUSTER and global imaging by IMAGE.

1.1 Before IMAGE and CLUSTER

Before the IMAGE and CLUSTER missions, structures in the plasmasphere with both large- and small-scale number density variations had been observed by OGO 5 (Chappell et al.

J.C. Foster
Haystack Observatory, Massachusetts Institute of Technology (MIT), Westford, MA, USA
e-mail: jfoster@haystack.mit.edu

J. Goldstein
Southwest Research Institute (SwRI), San Antonio, TX, USA
e-mail: jgoldstein@swri.edu

M.B. Moldwin
Institute of Geophysics and Planetary Physics (IGPP), University of California, Los Angeles, CA, USA
e-mail: mmoldwin@igpp.ucla.edu

B.W. Reinisch · J. Tu
Center for Atmospheric Research, University of Massachusetts-Lowell (UML), Lowell, MA, USA

B.W. Reinisch
e-mail: Bodo_Reinisch@uml.edu

J. Tu
e-mail: Jiannan_Tu@uml.edu

B.R. Sandel
Lunar and Planetary Laboratory (LPL), University of Arizona, Tucson, AZ, USA
e-mail: sandel@arizona.edu

1970b), by CRRES near the plasmapause (LeDocq et al. 1994), by geosynchronous satellites (Moldwin et al. 1995), and by various other ground-based and spacecraft instruments (see the review by Carpenter and Lemaire 1997).

Among those plasmaspheric density structures, large-scale features have been observed close to the plasmapause and to the plasmasphere boundary layer, PBL (Carpenter and Lemaire 2004). These structures are usually connected to the main body of the plasmasphere, and extend outwards. In the past they have been called "plasmaspheric tails" (e.g., Taylor et al. 1971; Horwitz et al. 1990) or "detached plasma elements" (e.g., Chappell 1974), since their topological relation to the main plasmasphere was not clear from single-satellite measurements. Those structures are now known as "plasmaspheric plumes" (e.g., Elphic et al. 1996; Ober et al. 1997; Sandel et al. 2001). Plumes have commonly been detected in the past by in situ measurements on satellites such as OGO 4 (Taylor et al. 1971), OGO 5 (Chappell et al. 1970a), ISEE-1 (Carpenter and Anderson 1992), CRRES (Moldwin et al. 2004; Summers et al. 2008), and several at geosynchronous orbit (Moldwin et al. 1995; Borovsky et al. 1998), but also by ground-based instruments (Carpenter et al. 1993; Su et al. 2001). Plumes were predicted on the basis of various theoretical models. When geomagnetic activity increases, the convection electric field intensifies, as the electric potential across the magnetosphere increases, driven by the interaction between the solar wind and the Earth's magnetosphere. The outer layer of the plasmasphere is stripped away, and the plasmasphere shrinks (Grebowsky 1970; Chen and Wolf 1972; Chen and Grebowsky 1974). This process is known as plasmaspheric erosion. The eroded plasma provides the material to form plasmaspheric plumes, which extend sunward. During storm recovery plumes become entrained in corotational motion, rotating eastward into the nightside inner magnetosphere. Numerical simulations using the Rice University model and the Magnetospheric Specification and Forecast Model reproduced the formation and motion of plumes (Spiro et al. 1981; Lambour et al. 1997). The interchange instability mechanism also predicts the formation of plasmaspheric plumes (Lemaire 1975, 2000; Pierrard and Lemaire 2004; Pierrard and Cabrera 2005.

Earlier in situ observations revealed a host of complex density structures at medium-scale (e.g., Horwitz et al. 1990; Carpenter et al. 2000). However, it was difficult to understand those structures without the context afforded by global imaging and multi-satellite missions. Small-scale density irregularities have also long been observed. In the early 1960s, the existence of narrow density irregularities extended along geomagnetic field lines was established (e.g., Smith 1961; Helliwell 1965). The irregularities were usually not detected directly, but instead were studied indirectly through their transmission properties as wave ducts or guides. Later satellite measurements revealed concentrations of cross-field density irregularities in the vicinity of the plasmapause, for example with the LANL geosynchronous satellites (Moldwin et al. 1995) or the CRRES spacecraft (Fung et al. 2000). Several mechanisms have been suggested to explain those small-scale density structures, like the drift wave instability (e.g., Hasegawa 1971), or the pressure gradient instability (e.g., Richmond 1973). Irregular density profiles are also predicted by plasmaspheric models that simulate the convection (erosion) and refilling processes, like the Convection-Driven Plasmaspheric Density Model (Galperin et al. 1997) and the Rice University model (Spiro et al. 1981). Theoretical modeling of plasmaspheric refilling was also found to produce density irregularities in the equatorial region (Singh 1988; Singh and Horwitz 1992). Turnings and changes of strength of the interplanetary magnetic field (IMF) influence the convection and might be responsible for the formation of density irregularities (Goldstein et al. 2002; Spasojević et al. 2003). Plasma interchange motion was shown to be able to create density irregularities (Lemaire 1974, 2001).

With new experimental perspectives come new physical insights. The IMAGE and CLUSTER missions have fundamentally changed our knowledge about plasmaspheric density structures. IMAGE has made remote, global observations with the Extreme UltraViolet (EUV) instrument (Sandel et al. 2000) and the Radio Plasma Imager (RPI) instrument (Reinisch et al. 2000), from points both outside and within the plasmasphere (e.g., Carpenter et al. 2002; Sandel et al. 2003). The CLUSTER satellites are making detailed and coordinated multipoint measurements in the outer plasmasphere using the WHISPER (Waves of HIgh frequency and Sounder for Probing Electron density by Relaxation) instrument (Décréau et al. 1997) and other instruments (e.g., Darrouzet et al. 2004; Dandouras et al. 2005; Décréau et al. 2005).

1.2 IMAGE Observations of Density Structures

From its initial high-latitude apogee the IMAGE spacecraft (Burch 2000) provided an excellent platform for remotely observing the azimuthal distribution of plasmaspheric plasma with the EUV instrument. Designed to detect solar-origin extreme ultraviolet light at 30.4 nm resonantly scattered by thermal He^+, EUV provided the first global images of the plasmasphere. At a time cadence of 10 minutes, EUV images were able to repeatedly follow plasmaspheric dynamics from storm onset and erosion through recovery and refilling. The resulting global view provided a new context for more than 40 years of in situ and ground observations. One of the first results led to a refinement in our descriptive language for plasmaspheric structures, which is presented in Fig. 1. The six EUV image panels provide examples of plumes, notches, shoulders, fingers, channels and crenulations. The shadows and aurora are not features of the plasmasphere, but are routinely present in the images. The brightness in these images is proportional to the line integral of the He^+ abundance along each pixel's line of sight.

Like for EUV, the RPI instrument provides an entirely new perspective on thermal plasma density structures. RPI measured inner magnetospheric electron densities both actively and passively. The passive electric field measurements are used to observe natural radio noise and to derive electron densities local to the spacecraft as has been done with all previous in

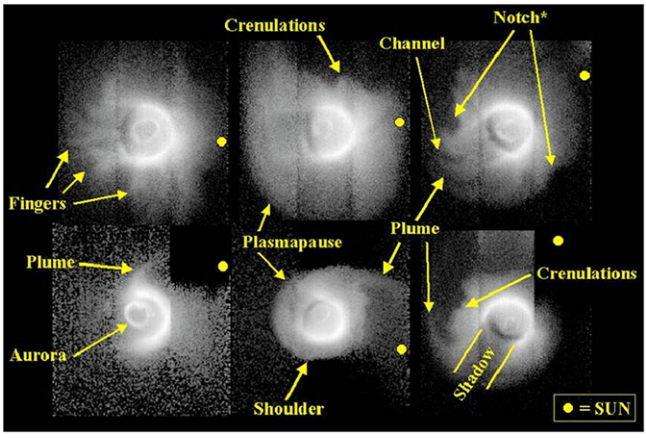

Fig. 1 Structures observed by the EUV instrument onboard IMAGE and new morphological nomenclature: examples of shoulders, plumes, fingers, channels, crenulations and notches. The direction to the Sun is shown as a *yellow dot* for each image. (From http://image.gsfc.nasa.gov/poetry/discoveries/N47big.jpg)

situ plasma wave instruments, except with greater sensitivity due to the long 500 m cross dipole antenna in the spacecraft spin plane. A 20 m tip-to-tip antenna was deployed along the spin axis to complete the 3-axis electric field antenna system. RPI actively broadcast digitally coded signals from 3 kHz to 3 MHz in order to quantitatively sample remote electron densities from about 0.1 to 10^5 cm^{-3} through the returned echoes. Thousands of plasmapause crossings and field-aligned density distributions with resolution better than 1 minute in time, 0.1 R_E in range, and 10% in density have been obtained and are still being analyzed.

Those instruments and related tools are described in more detail elsewhere in this issue (De Keyser et al. 2008).

1.3 CLUSTER Observations of Density Structures

In contrast with IMAGE, which provides global two-dimensional (2-D) views of the plasmasphere in a large domain of local time (LT) and geocentric distance (R), CLUSTER provides a meridian view of plasmaspheric density, by way of four orbital sweeps placed within a limited range in LT and R, as the four CLUSTER spacecraft (C1, C2, C3, C4) cross the plasmasphere near perigee around 4 Earth radii (R_E) every 57 hours from southern to northern hemisphere (Escoubet et al. 1997). Figure 2a displays a three-dimensional (3-D) view of the CLUSTER orbits during such a crossing. Each spacecraft provides a density profile versus s, the curvilinear distance along track. The two main parameters, latitude λ and McIlwain L parameter (McIlwain 1961), are explored in a coupled way along the orbit. More precisely, electron density n_e is obtained from the WHISPER instrument (Décréau et al. 1997, 2001), which in its active mode, unambiguously identifies the electron plasma frequency f_{pe} (Trotignon et al. 2003), directly related to n_e. f_{pe} can also be inferred from WHISPER passive measurements by estimating the low frequency cut-off of natural plasma emissions (Canu et al. 2001). WHISPER operates between 2 and 80 kHz, with a frequency resolution of 163 Hz. This corresponds to densities between 0.05 and 80 cm^{-3}, with a relative precision that varies from 16% for low densities to 0.4% for high densities. The time resolution of density measurements is $\lesssim$3 s, corresponding to a distance along the orbit of $\Delta s \lesssim 15$ km. More precisely, the WHISPER instruments deliver four density profiles,

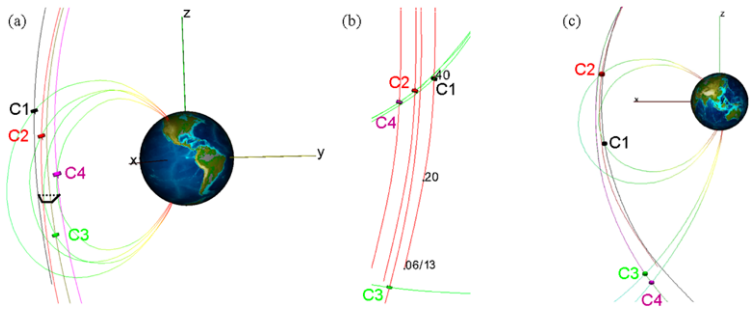

Fig. 2 **a** Instantaneous view of the four CLUSTER satellites during the ~5000 km separation season (September 2002). The section of the tube limited by the four orbital paths is outlined. **b** "Field-aligned" configuration in a tail season (June 2001). For the trio C1–C2–C4, the largest separation distance is ~2000 km along field lines, the smallest being ~200 km across field lines. C3 is placed at ~9000 km from the trio. **c** Multi-scale configuration in a tail season (August 2005). Figure produced with the Orbit Visualisation Tool (OVT, http://ovt.irfu.se)

$n_e^i(s_i)$, i from 1 to 4, versus respective distances s_i along orbits. This provides a spatio-temporal sampling of the region explored, as s_i depends on universal time (UT) and position (LT, L, λ).

Such density profiles obtained from single-satellite missions like GEOS, ISEE, DE and CRRES, have generally been analyzed by focusing on one variable, mostly L (e.g., Carpenter and Anderson 1992), sometimes λ (e.g., Décréau et al. 1986), or LT for geosynchronous satellites, by assuming either uniformity of density over the explored range of the three other quantities, or by using other models of spatio-temporal density variations. CLUSTER provides new perspectives in plasmasphere observations, not only thanks to an unprecedented spatial resolution and to accurate density measurements by WHISPER, but also because density profiles can be compared to each other in order to test models and to study the 3-D view and the lifetimes of density structures.

In addition to plasma density, the multipoint measurements performed by the CLUSTER spacecraft in the plasmasphere provide other parameters such as the plasma composition and 3-D ion distribution functions measured by the Cluster Ion Spectrometry (CIS) experiment (Rème et al. 2001), or the electric field measured by the Electric Field and Wave (EFW) instrument (Gustafsson et al. 2001) and the Electron Drift Instrument (EDI), (Paschmann et al. 2001). Those instruments and related tools are described in more detail elsewhere in this issue (De Keyser et al. 2008).

The changes in the CLUSTER configuration (spacecraft separation varies from 100 to 10000 km) and the evolution of its orbit over the years, coupled to the natural dynamics of the plasmasphere, enable a variety of scientific questions to be addressed. Small spacecraft separations (100 km) allow small-scale structures to be resolved (Décréau et al. 2005; Darrouzet et al. 2004, 2006a), while large ones (5000 km), which are associated with larger time shifts, can be used to assess lifetime of structures or to address global dynamics (Darrouzet et al. 2008). All constellations are elongated along the orbit track, a property which can be turned into an advantage, since many of the smallest-scale structures are field-aligned. Spacecraft can be magnetically conjugate, either in a loose way (Fig. 2a), where C2 in the northern hemisphere and C3 in the southern hemisphere are at close transverse distance ($\sim$500 km) from the same magnetic field line, or in a more tight way (Fig. 2b), where three satellites are grouped along the same magnetic field line, at small transverse distances ($\sim$200 km). Lastly, the multi-scale configuration (Fig. 2c) can be used to study small-scale evolutions in a context simultaneously explored at a larger scale.

1.4 Outline of the Paper

The purpose of this paper is to survey the results obtained with CLUSTER and IMAGE on plasmaspheric density structures. Section 2 presents a new vision of the erosion and refilling processes, and new results about the plasmaspheric wind. The overall plasma distribution in the plasmasphere and several studies about the plasmapause are described in Sect. 3. Section 4 presents various results on the ion composition of the plasmasphere. The four following sections are devoted to studies of specific types of density structures, from large-scale to small-scale: plasmaspheric plumes in Sect. 5, notches in Sect. 6, other medium-scale density structures in Sect. 7, and small-scale density irregularities in Sect. 8. Section 9 concludes the paper and offers an outlook.

2 Sources and Losses in the Plasmasphere

It is well known that the plasmasphere is very dynamic, constantly in a state of change, contracting and eroding in a few hours in response to increasing geomagnetic activity and refilling over a period of a few days in quiet times. Both processes received much experimental and theoretical attention (e.g., Lemaire and Gringauz 1998), but the advent of the CLUSTER and IMAGE missions played an important role in the study of those processes, which contribute to the sources and losses of plasma in the plasmasphere.

2.1 The Disturbed Plasmasphere: A New Look at Refilling

Dynamic exchange typifies the ion populations of the plasmasphere and ionosphere and this flux is an important aspect of their coupling. Roughly speaking, the daylit portion of ionosphere supplies material to the plasmasphere, while the flow direction is into the dark ionosphere. This diurnal variation is often overwhelmed by more pronounced sinks of plasmaspheric ions, such as erosion of the entire outer plasmasphere. Following erosion events, the dominant trend in the plasmasphere is towards increasing densities and this trend is termed refilling.

Refilling of the plasmasphere has been studied for many years using ground-based and in situ techniques, but this section focuses on new results based on IMAGE data. Sandel and Denton (2007) developed a global view of refilling, using EUV observations taken onboard IMAGE. They studied the azimuthally-averaged change of He^+ column densities and equatorial abundances during an unusually quiet period extending for about 70 hours. Geomagnetic conditions during this time suggest that losses of plasmaspheric material due to erosion were minimal, leading to measurements of refilling that were expected to be largely uncompromised by confounding effects. By computing azimuthal averages of summed EUV images, Sandel and Denton (2007) derived radial profiles of He^+ column abundance at six times during the study interval corresponding to six consecutive IMAGE orbits. These profiles showed an orderly increase in column abundance with time, which slowed near the end of the period.

Instead of doing a global study of refilling, Gallagher et al. (2005) studied a small region of particular interest. They reported the first measurements of refilling using EUV observations. They were particularly interested in the physics governing the formation and evolution of plasmaspheric notches, so their measurements of refilling were made in such a feature. By tracking a notch over three IMAGE orbits, they avoided errors that could have been introduced by deviations from perfect corotation (see Sect. 6). Binning in radial distance yielded measurements at three L-positions at the single azimuth defined by the notch, which drifted relative to corotation. Geomagnetic conditions varied during the interval of their study, leading to increasing He^+ abundance during two of the orbits and decreasing abundance during the intervening orbit. Considering only the times and distances for which refilling was unambiguous, Gallagher et al. (2005) found averaged refilling rates at the equator of 3.8 He^+ $cm^{-3}\,h^{-1}$ at $L = 2.75$ and 2.7 He^+ $cm^{-3}\,h^{-1}$ at $L = 3.25$. These rates represent a limited sample of space and time, but are higher than would be expected on the basis of many other measurements, which for comparison often must be extrapolated in L and further are at best an indirect measure of the He^+ refilling rate.

Whereas the fundamental quantity measured by EUV was the change in He^+ column abundance with L and time, measured or modelled refilling is usually reported in terms of volume rates. For more direct comparison with these measurements and models, Sandel and

Denton (2007) used the method described by Gallagher et al. (2005) to convert He^+ column abundances to equatorial volume abundances; then converting to volume refilling rates was straightforward. The inferred refilling rate at the equator, averaged over the 69-hour study period, decreases with L, from 1 He^+ cm^{-3} h^{-1} at $L = 2.3$ to 0.07 He^+ cm^{-3} h^{-1} at $L = 6.3$. The rates determined in this way are generally a factor of 3–4 lower that those inferred by Gallagher et al. (2005) at corresponding values of L. This difference is not surprising given that the determination of Sandel and Denton (2007) uses averaging over a much longer time, and consequently includes the slower approach to saturation.

Further, other measurements and models refer to species other than He^+, such as electron densities or total ion mass. For comparing with these determinations, Sandel and Denton (2007) used estimates of the variation of the ratio α between the He^+ density and the H^+ density with L (Craven et al. 1997), and, where necessary, neglected the contribution of heavier ions to the plasmaspheric mass density. With these approximations, they found their measurements to have a radial dependence similar to that inferred from earlier measurements and models, but their absolute values for refilling rates were generally higher by a factor of 4. They mention two factors that may contribute to this difference: (i) extrapolating the radial dependence of the ratio α outside the domain over which it was originally defined; (ii) possible interspecies variations in the refilling rate with time and L.

In spite of the uncertainties that arise when using observations of He^+ as a proxy for plasmaspheric particle populations, the global view provided by remote sensing offers advantages over more traditional techniques. These include sensing all LT and radial distances simultaneously, and avoiding errors possible when density changes driven by, i.e., departures from corotation are interpreted as purely temporal.

Galvan et al. (2008) used EUV to investigate the diurnal variation in He^+ column abundance, thus extending refilling studies to shorter timescales. Their work is unique in investigations of the diurnal variation, in that it relates to heavy ions rather than electrons or protons, and that by tracking brightness features in the plasmasphere they were able to account for departures from corotation to accurately follow a specific volume element of plasma. Their analysis of over 1000 EUV images from 128 IMAGE orbits revealed a consistent picture of the diurnal variation: (i) a general increase in He^+ abundance from dawn to dusk, peaking shortly after dusk at a level higher than dawn by a factor of 1.5–2; (ii) a region near noon where abundances remain constant or decrease slightly. They report similar behaviour in relative rates at $L = 2.5$ and 3.5. The absolute rates of change in abundance at the two distances were consistent with the difference in flux tube volume, assuming similar rates of supply from the ionosphere at the two latitudes. The measured variations show no dependence on geomagnetic activity, but were consistent with the idea that the diurnal variation in He^+ abundance is dominated by upflow from the sunlit ionosphere and downflow into the night ionosphere.

Complementary to line-of-sight global measurements of the EUV instrument, sounding measurements from the RPI instrument provided field-aligned electron density profiles that are almost instantaneously obtained. Multiple field-aligned density profiles were sometimes available along an extended portion of the IMAGE orbit. As a consequence, 2-D electron density images can be constructed (Tu et al. 2005). It allows to infer plasma dynamics from RPI 2-D density profiles, such as plasma refilling in the outer plasmasphere and plasma acceleration in the aurora/cusp region. Those density profiles provide the first true magnetospheric electron density gradient along magnetic field lines, which has not previously been practical using in situ measurements. If the local production and loss of the charged particles are assumed small (true for the plasmasphere and subauroral trough), if plasma transport across magnetic field lines is neglected, and assuming quasi-steady conditions, the electron number

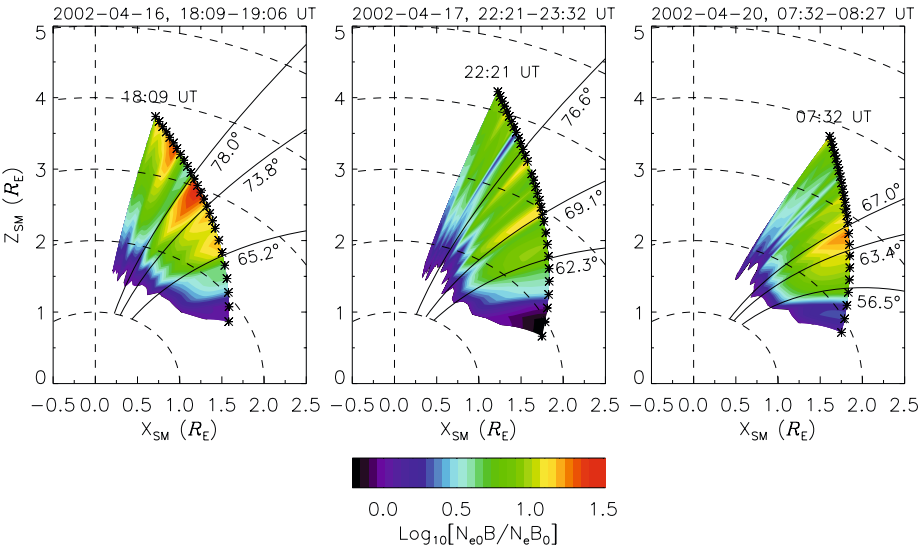

Fig. 3 Two-dimensional images of the normalized field-aligned electron velocity, projected onto the solar magnetic (SM) X_{SM}–Z_{SM} plane and derived from the field-aligned density profiles measured by RPI on three different days. The *stars* on each orbit segment indicate the locations from which the field-aligned density profiles were measured. Three field lines (*solid*) are plotted with the corrected geomagnetic coordinate (CGM) latitude labeled. The field line of lowest latitude indicates the plasmapause, while the two other delimit a density depletion region. (Adapted from Tu et al. 2005)

flux is conserved along magnetic field lines. Variations of the electron velocity parallel to magnetic field lines can thus be derived. Figure 3 displays for three different days 2-D images of this velocity normalized by the electron velocity at the base of the individual electron density profiles. Several regions of different velocity characteristics can be identified from this figure. In the inner plasmasphere the normalized electron velocity is almost constant along field lines. Beyond the plasmapause, in the trough region, the normalized velocities rapidly increase along the field lines at altitudes above about 1 R_E, indicating a possible plasma acceleration above this altitude.

2.2 The Quiet Plasmasphere

Attention is most often paid to the striking plasmaspheric density structures produced during disturbed geomagnetic conditions. Plasmaspheric plumes, notches, and plasmapause undulations dominated our studies of plasmaspheric physical processes. Unlike the slow, multiple day process of plasmasphere refilling, these processes unfold in minutes to hours. The consequence is that other, more subtle physical processes have often been overlooked. However, the PLANET-B, IMAGE, and CLUSTER missions recently led to discoveries that have significant implications for the modelling of the quiet plasmasphere, providing us with new opportunities to study the mechanisms of plasmapause formation, in particular when there are no confounding effects associated with disturbed geomagnetic periods (e.g., Yoshikawa et al. 2003; Tu et al. 2007).

Extended quiet periods, i.e., when the geomagnetic activity index K_p is low (such as $<1^+$), are required to allow refilling to significantly proceed, especially at geosynchronous orbit and beyond where refilling times are expected to be many days. Such periods are most likely to exist during solar minimum. Reynolds et al. (2003) recently listed the yearly

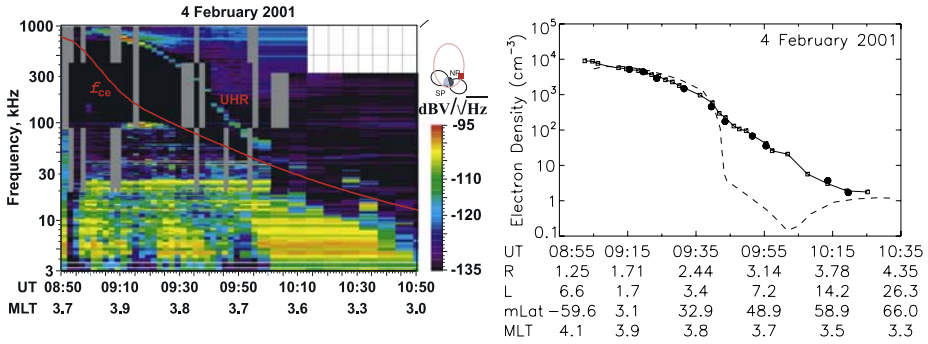

Fig. 4 (*Left*) Electric field spectrogram measured by RPI showing an upper hybrid resonance (UHR) band. The *red line* is the electron gyrofrequency determined from the Tsyganenko and Stern (1996) model. The gray strips indicate frequencies and times when no passive data were measured from RPI. The IMAGE orbit configuration is displayed on the *upper right corner*. (*Right*) Electron densities derived from the lower frequency cutoff of the UHR band along the IMAGE orbit. The *dashed line* represents electron densities from the empirical model of Gallagher et al. (2000). The *solid dots* are in situ electron densities derived from the available sounding measurements. (Adapted from Tu et al. 2007)

occurrence frequencies of various lengths of quiet periods for the entire 69-year history of recorded K_p values (from January 1932 to December 2000). It can be seen from their study that quiet time periods longer than two days with $K_p \leq 0^+$ occur rarely, but periods with $K_p \leq 2^-$ occur approximately 14 times per year.

The plasmasphere rarely appears filled to saturation, i.e., in diffusive equilibrium with the ionosphere. Tarcsai (1985) reported that the day-to-day filling of the plasmasphere after magnetic disturbances continues several days without exhibiting saturation levels corresponding to diffusive equilibrium, even for radial distances deep inside the plasmasphere. More recent observations found significant refilling in less than 28 hours near $R = 2.5\ R_E$ (Reinisch et al. 2004), but still insufficient to reach saturation levels. Reynolds et al. (2003) compared locally measured plasma densities with theoretical predictions obtained from a multispecies kinetic model. The observed density level was at most only 25% of saturation density, and the density still appeared to increase even after three days of very quiet geomagnetic activity. In addition, according to the Carpenter and Anderson (1992) empirical model for saturated equatorial densities, the averaged slope of the logarithmic density is found to be independent of radial distance inside 8 R_E, which does not correspond to that expected for a plasmasphere in diffusive equilibrium (see Fig. 8 in Pierrard et al. 2008, this issue). Beyond the limited time permitted for the plasmasphere to reach saturation, some researchers suggest refilling is slower than expected due to an additional process at work.

After many days of very quiet geomagnetic conditions, a distinct plasmapause boundary may not be found, particularly on the dayside of the Earth. Such a boundary is expected as a consequence of the continued presence of solar wind induced convection at high latitudes. Nevertheless, prolonged quiet-time observations have found smooth plasmasphere density variations extended to about $L = 7$ or beyond (e.g., Chappell 1972; Carpenter and Anderson 1992; Tu et al. 2006), implying an extended plasmasphere with either the plasmapause located beyond $L = 7$ or a smooth density transition to the subauroral region without a clear plasmapause signature. Such a smooth transition is possible if magnetospheric convection is very weak so that corotation dominates to a large radial distance. Tu et al. (2007), using passive measurements from RPI, present cases of a smooth electron density transition from the plasmasphere to the subauroral region without a signa-

ture of the plasmapause. Figure 4, as an example, displays a smooth transition as represented by the smooth frequency variations of the upper hybrid resonance (UHR) noise band (left panel) and the corresponding derived electron density (right panel). Such smooth transitions can occur at various MLT and were observed after geomagnetic activity had been quiet for 2 or more days, with K_p primarily less than 3 for the cases examined. The survey of the RPI database indicates that such events occurred about 10% of the time.

2.3 New Evidence for a Plasmaspheric Wind

The unexpectedly long time for refilling and lack of a distinct plasmapause could be explained if the plasmasphere experiences a slow outward drift in addition to corotation and convection. Lemaire and Schunk (1992, 1994) noted that it would then take more time to refill a flux tube when it is lost through an outward drift across magnetic field lines in the form of a plasmaspheric wind. This concept is based on the result of plasma interchange motion, which is driven by an imbalance between pressure gradient and gravitational, centrifugal and inertial forces (André and Lemaire 2006). This outward drift is also controlled by the height-integrated Pedersen conductivity of the ionosphere.

Global imaging recently demonstrated that plasmaspheric losses from the plasmaspheric wind are as significant as ionospheric refilling, for populating the region just outwards of the plasmapause, even under quiet/moderate geomagnetic condition (Yoshikawa et al. 2003). At the plasmapause, the smooth electron density transition from the plasmasphere to the subauroral region observed by RPI was interpreted by Tu et al. (2007) as additional indirect evidence for a plasmaspheric wind.

A recent analysis of ion distribution functions acquired in the outer plasmasphere by CIS revealed a significant anisotropy in the particle fluxes. Systematically more ions are going outwards than inwards in the plasmasphere at all LT. This may constitute the first direct evidence for a continuous escape of plasma from the plasmasphere, the plasmaspheric wind (Dandouras 2008). The contribution of this plasmaspheric wind to plasma populations outside the plasmasphere is not negligible, with preliminary estimates indicating that it could be of the same order as the solar wind input to the magnetosphere under quiet geomagnetic conditions.

2.4 Erosion of the Plasmasphere

The storm-time loss of plasma in the outer plasmasphere, or plasmaspheric erosion, is one of the oldest known properties of the plasmasphere (Gringauz et al. 1960; Carpenter 1962). Early on, the location of the plasmapause was associated with the last closed equipotential resulting from the superposition of the corotation and convection electric fields. Its erosion or inward motion was found to occur with increased geomagnetic activity and was modeled by a corresponding increase in the convection electric field (Nishida 1966). An inward motion of plasma and steepening of the plasmapause has also been associated with the consequences of the dynamic balance between centrifugal and other forces (Lemaire 1974, 1985).

Global images have revealed the morphology of the plasmaspheric response to changes in convection. IMAGE observations show that the overall erosion process starts with a slight initial indentation in the plasmasphere near midnight that widens and spreads eastward and westward, encompassing the entire nightside plasmasphere within a few hours (Spasojević et al. 2003; Goldstein et al. 2003a; Goldstein and Sandel 2005; Gallagher and Adrian 2007). The basic pattern of erosion and formation of the plasmaspheric plume is illustrated using

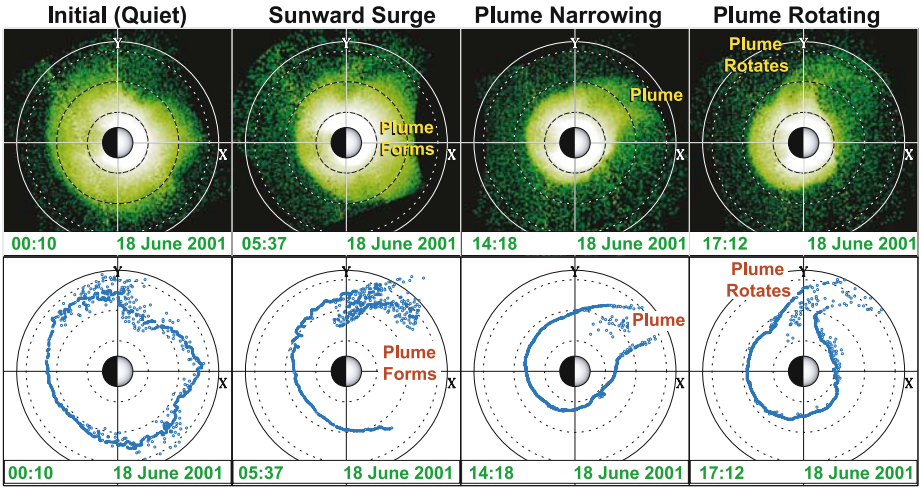

Fig. 5 (*Top row*) EUV plasmasphere images on 18 June 2001, depicting erosion of the plasmasphere and formation and rotation of a plume. Each panel displays the equatorial plasmaspheric He^+ distribution versus X and Y (in SM coordinates). *Color* indicates column abundance (in arbitrary units). The Sun is to the right (positive X) and the Earth is the *half-shaded circle* in the center. *Dotted circles* are drawn at $L = 2$, 4, and 6; the *solid circle* indicates geosynchronous orbit. (*Bottom row*) The *blue circles* are manually extracted points from the EUV image directly above, showing the outer boundary of the plasmasphere. (Adapted from Goldstein 2006)

EUV observations in Fig. 5. Erosion for this 18 June 2001 event follows a southward turning of the IMF. It shows the typical pattern of initial night-time plasmaspheric loss and broad dayside plume formation, followed by a narrowing of the plume as erosion nears an end and associated with its rotation eastward (see Goldstein 2006). Driven by an enhanced solar wind electric field, the onset of erosion requires 10–30 minutes to propagate from the magnetopause to the inner magnetosphere through the ionosphere (Goldstein et al. 2003a; Murakami et al. 2007). RPI observations also demonstrate the dramatic loss of plasma along magnetic field lines (Reinisch et al. 2004). Outer plasmaspheric flux tubes lost more than two thirds of their plasma in less than 14 hours during the 31 March 2001 storm. Later recovery of the plasmasphere by refilling occurred over a period of 10 days.

In this process, removal of plasma occurs at different times for different MLTs, so that the effects of erosion propagate with a finite speed, eastward and westward from the initial MLT where erosion is first observed. This finite propagation effect has been observed in every erosion event for which EUV data have been analyzed (Spasojević et al. 2003; Goldstein et al. 2003a; Goldstein and Sandel 2005). A similar finite propagation effect occurs during transient disturbances of the plasmapause, such as the so-called plasmapause undulations produced by bursts of convection associated with substorms (Goldstein et al. 2004a, 2005a, 2007). A plasmapause undulation event is part of a chain of interconnected electrodynamic and plasma phenomena. First, substorm dipolarization injects plasma into the ring current, inflating the geomagnetic field, inducing an electric field which pulls the plasmapause outward to form a 1–2 R_E bulge. Ionospheric closure of the partial ring current then generates a westward subauroral polarization stream (SAPS) flow that removes the 1–2 R_E bulge. The net global effect is an outward-then-inward motion that propagates westward along the plasmapause. This westward-moving undulation, accompanied by a smaller, subtler eastward-moving ripple, can be correlated with corresponding intensifications of the aurora to a greater or lesser degree (Goldstein et al. 2005a, 2007).

3 Overall Plasma Distribution and Plasmapause Position

As discussed above, the IMAGE and CLUSTER missions provided us with a new appreciation of the plasmasphere through global and multipoint plasmaspheric observations. The overall geometry and context of the time varying distribution of plasmaspheric plasma has been revealed in ways not previously possible.

3.1 Overall View from EUV

The global images obtained from EUV onboard IMAGE provide an overall view of the plasmasphere. They can be used to infer the plasmapause position, by looking at the He^+ edge, i.e., the outermost sharp edge where the brightness of He^+ emissions drops abruptly (Goldstein et al. 2003b). On EUV images, many density structures appear as seen in Fig. 1. Successive images illustrate the spatial and temporal evolution of such structures. For example, undulations of the plasmapause can be observed and an equatorial azimuthal speed of such structure can be deduced: 4 $R_E\,h^{-1}$ at $L = 4$ in a case event analysed by Goldstein et al. (2004b).

3.2 Plasma Density in the Plasmasphere

The sounding measurements from RPI onboard IMAGE provided field-aligned electron density profiles that are almost instantaneously obtained (Reinisch et al. 2000). 2-D electron density images along the satellite orbit can be constructed with those multiple density profiles. Such images proved to be useful to differentiate various plasma regions in the near Earth magnetosphere and to provide insights to the plasma dynamics in those regions. Tu et al. (2005) presented case studies of three electron density images obtained before, during and after a magnetic storm. Figure 6 displays the images on three separate days of field-aligned electron density divided by r^{-5}, where r is the radial distance along individual field

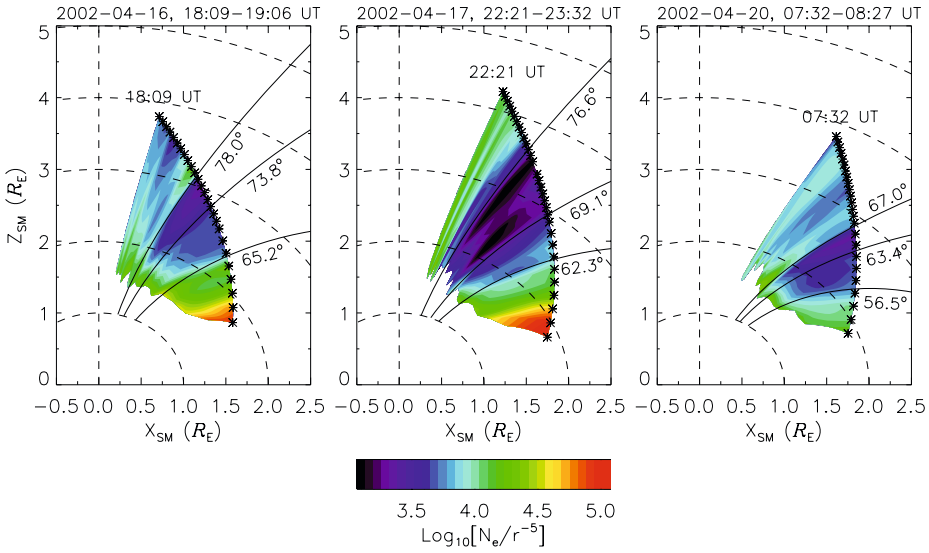

Fig. 6 Same format as Fig. 3 but for electron density images divided by r^{-5}, where r is the radial distance (in R_E) along individual field lines. (Adapted from Tu et al. 2005)

lines. Such normalization is useful since the densities in different plasma regions have a distinct radial distance dependence; it helps to better differentiate the plasma regions relative to the polar cap. The RPI observations allow plasma regions to be identified more reliably because their 2-D spatial extent can be seen. Furthermore, the difference in the radial dependence of the densities along field lines in these regions can be determined using the near instantaneously measured field-aligned density profiles. The plasma regions, namely, the plasmasphere, plasmatrough, V-shaped density depletion region, cusp, and polar cap are clearly differentiated in the images because the polar cap density variations along field lines are nearly proportional to r^{-5} (Nsumei et al. 2003, 2008), as demonstrated by Fig. 6. For example, the plasmasphere is shown consisting of two layers: the high-density region mentioned above, and a high-L region with lower densities.

3.3 Overall Density Gradients in the Plasmasphere

Darrouzet et al. (2006b) and De Keyser et al. (2007) analyzed a plasmasphere pass by CLUSTER to study the overall geometry of the plasmaspheric density structure, using gradient computation techniques. Such a study is only possible with high precision data, which is achieved with the electron density n_e determined from WHISPER. Techniques to compute the gradients along the trajectory of CLUSTER are described elsewhere in this issue (De Keyser et al. 2008). A fundamental requirement for these methods is the hypothesis that the satellites are close enough to each other, so that all spacecraft are embedded in the same structure at the same time (homogeneity condition).

Darrouzet et al. (2006b) analyzed the plasmasphere pass on 7 August 2003, at 14:00 LT and between $-30°$ and $+30°$ of magnetic latitude $MLAT$. The maximum value of K_p in the previous 24 hours was 2^+. The spacecraft separation was small and the tetrahedron geometric factors are satisfactory. Figure 7a illustrates that the WHISPER density differences between the four satellites vary as a function of time. The density gradient ∇n_e on the inbound crossing is generally towards Earth, with some azimuthal deviations. During the outbound crossing, ∇n_e behaves less regularly. Interesting insights can be gained by analysing the angle $\alpha_{\boldsymbol{B},\nabla n_e}$ between the magnetic field vector $\boldsymbol{B}$ and the density gradient ∇n_e at the center of the tetrahedron (see Fig. 7b). The global orientation of the density gradient can also be described by its latitude $\theta_{\nabla n_e}$ (blue curve in Fig. 7c) and its azimuth relative to the spacecraft azimuth angle $\phi_{\nabla n_e} - \phi_{\rm sc}$ (red curve in Fig. 7c). Figure 7 displays those angles obtained with the classical gradient method (Darrouzet et al. 2006b); comparable results have been found with the least-squares gradient method (De Keyser et al. 2007).

In regions A, C and E, the density changes rather slowly (Fig. 7a) and the three angles displayed on Figs. 7b–c demonstrate that the density structures are largely cylinder-symmetric, but with the presence of azimuthal ripples, which are similar to the structures described by Bullough and Sagredo (1970). When the spacecraft observe markedly different densities at a given time (regions B and D on Fig. 7a), the density gradients are definitely stronger. This is due to the presence of field-aligned density structures, i.e., steep density changes across field lines (as illustrated by the angles displayed on Figs. 7b–c). The corresponding geometry in the equatorial plane is sketched in Fig. 8: The density gradient is inward during the inbound crossing; it points azimuthally duskward for much of the outbound one. The thicknesses of these density steps (500 to 1000 km) are sufficiently large so that the homogeneity condition is satisfied: The gradient computation produces correct results.

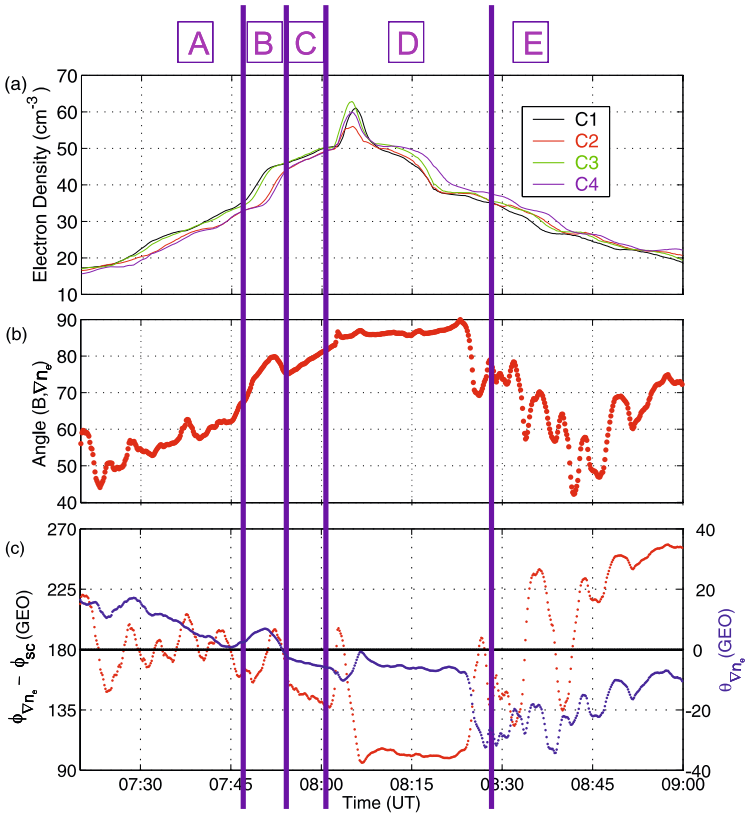

Fig. 7 **a** Electron density from WHISPER for the four CLUSTER spacecraft, **b** angle $\alpha_{\boldsymbol{B},\nabla n_e}$ between the magnetic field vector $\boldsymbol{B}$ and the density gradient ∇n_e, **c** latitude angle $\theta_{\nabla n_e}$ (*blue curve*), and azimuth angle of ∇n_e relative to the spacecraft azimuth, $\phi_{\nabla n_e} - \phi_{\rm sc}$ (*red curve*), as a function of time during the plasmasphere pass on 7 August 2003. The angles are known up to about 9°. (Adapted from Darrouzet et al. 2006b)

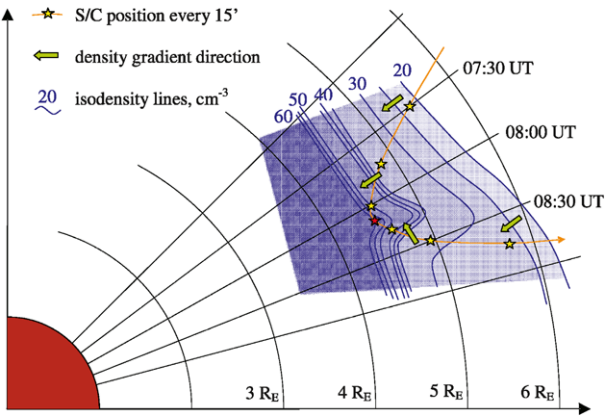

Fig. 8 Sketch of the plasmasphere pass on 7 August 2003 projected onto the equatorial plane in a corotating frame, chosen so that the perigee pass (at about 08:00 UT) corresponds to the LT at perigee (about 14:00 LT). (Adapted from Darrouzet et al. 2006b)

3.4 The Plasmapause Seen by CLUSTER

3.4.1 Introduction

The structure of interest at the largest scales is the plasmasphere itself, and its outer boundary, the plasmapause. In the past, many studies focused on the equatorial plasmapause radial position as a function of LT and geophysical conditions (Lemaire and Gringauz 1998). From a CLUSTER perspective, a systematic study on this topic has yet to be undertaken. Three combined difficulties are encountered: (i) the range in L values when at small latitudes ($<20°$) is narrow (a window $\Delta L \approx 2$ at a central value decreasing from $L \approx 5$ at the start of the mission down to $L \approx 3.5$ at the end of the mission); (ii) the density range measurable by WHISPER (0.25–80 cm^{-3}) is below values encountered at inner plasmapause boundaries; (iii) the plasmapause is located inward from CLUSTER perigee in a number of events encountered during the first half of the mission. The second and third difficulties are less problematic in the day and dusk sectors, where the plasmasphere extends further outward, and can thus be crossed more often by the CLUSTER spacecraft at densities within the sounder's range. Clear plasmapause density gradients are regularly encountered in those sectors. Examples of such plasmapause crossings are visible in Fig. 9a, obtained in the noon sector at 5000 km spacecraft separation during a quasi-steady event (configuration displayed in Fig. 2a). Spectrograms display plasma frequencies (light blue emissions) measured by each of the four WHISPER instruments. The behaviour of the four density profiles corresponds to cuts of the plasmasphere at increasing geocentric distances from C4 to C3, C2 and C1, leading to decreasing time intervals spent by the respective satellites inside the inner plasmasphere (when f_{pe} is above the 80 kHz threshold), and increasing latitudes where the boundary is encountered. For this event, seven clear-cut plasmapauses associated with sharp

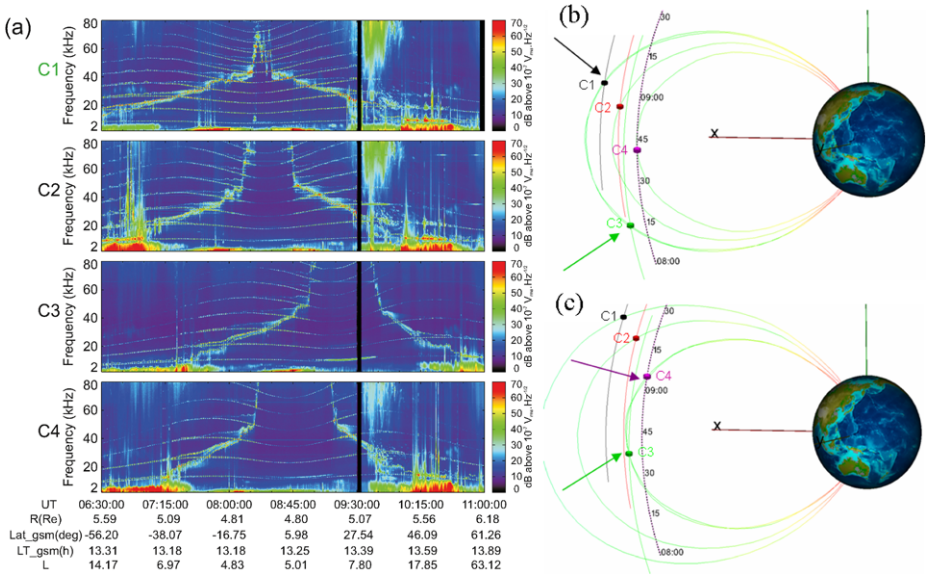

Fig. 9 **a** Time–frequency electric field spectrograms measured by the WHISPER instruments onboard the four CLUSTER satellites during a plasmaspheric pass on 15 August 2002 with a spacecraft separation around 5000 km. The orbital parameters correspond to C1. Examples of magnetic conjunction, **b** at 08:45 UT in the outer plasmasphere for C1 and C3, **c** at 09:06 UT in the inner plasmasphere for C3 and C4

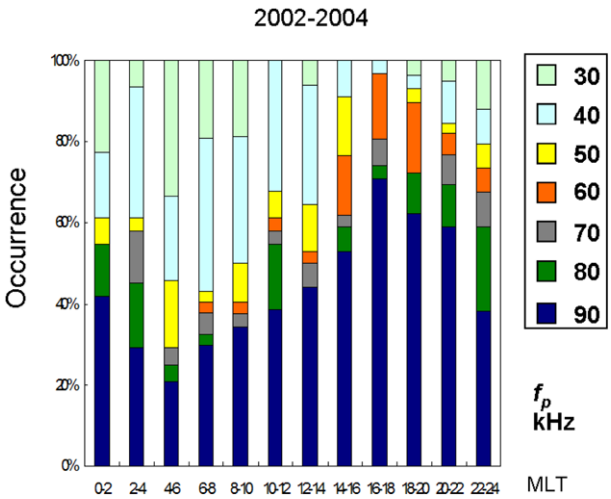

Fig. 10 Relative occurrence of equatorial plasma frequency values measured by WHISPER onboard CLUSTER in the different MLT sectors. (Adapted from El-Lemdani Mazouz et al. 2008)

local density gradients are observed with a plasma frequency increasing from ∼50 kHz (or a density ∼30 cm^{-3}). Those plasmapause crossings are seen by all spacecraft, except during the outbound pass of C1, which is associated with large-scale density fluctuations that complicate the identification of the plasmapause. All seven clear plasmapause crossings are placed within a narrow interval of L values (4.67 ± 0.10). Spacecraft are magnetically conjugate on six successive pairs during such events, at various latitudes (see examples in Figs. 9b–c), providing useful information about instantaneous latitudinal profiles. A full latitudinal density profile can further be obtained by a best fit with an empirical density model (Denton et al. 2008).

3.4.2 Statistical Study of the Plasmapause Distance

Despite the above quoted limitations of WHISPER density measurements, a systematic study of the plasmapause position in the equatorial plane has been conducted with CLUSTER, based on observations in years 2002–2004 (El-Lemdani Mazouz et al. 2008). Instead of searching for plasmapause boundary positions, the strategy has been to focus on the plasma frequency observed at the equator crossing on each CLUSTER orbit, a crossing located within a narrow geocentric window (4.2–4.7 R_E). By comparison with the empirical model of the plasmapause position given by Carpenter (1970), this plasma frequency gives a qualitative empirical estimate of the plasmapause distance to perigee. Figure 10 results from a study of 387 perigee events well distributed as a function of MLT. The plasma frequency figure is what has been measured (in bins of 10 kHz wide), except for the 90 kHz figure, indicating cases where the equatorial plasma frequency is higher than the upper range measurable by WHISPER. The highest occurrence of low frequencies is observed in the dawn (02:00–04:00 MLT) sector, while the high frequencies are observed mostly in the dusk (16:00–18:00 MLT) sector. This study is thus consistent with the expected dawn-dusk asymmetry of the plasmapause.

3.4.3 Plasmapause Dynamics: Position and Velocity

In the event of 15 August 2002 presented above (Fig. 9), a total of seven plasmapause positions have been identified within a narrow interval of L values, $\Delta L = 0.1$. Those measure-

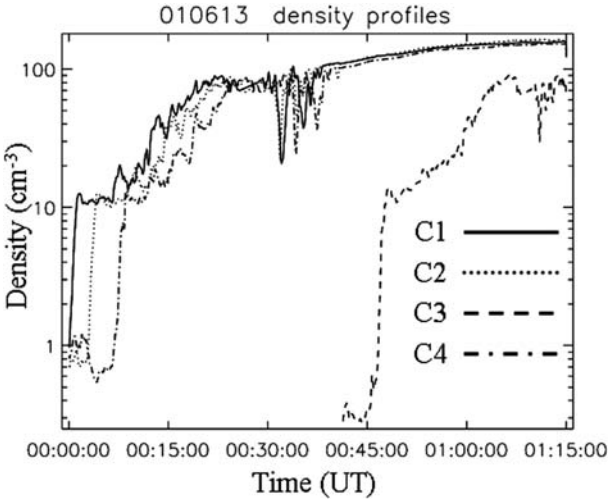

Fig. 11 Density profiles at the inbound perigee pass on 13 June 2001 determined by WHISPER onboard the four CLUSTER satellites. The plasmapause boundary (density step from 1 to 10 cm^{-3}) is crossed successively by C1, C2, C4 and C3. (Adapted from Décréau et al. 2005)

ments are spread over a time interval of 90 minutes, indicating that this boundary is quasi-stationary during the duration of the interval, within the MLT sector considered (around 13:00 MLT). In this example, the crossing points are placed at large distances from each other, over a large latitude interval.

When the crossing points are at close distance from each other ($<0.2\ R_E$), the plasmapause boundary can be considered locally as a magnetic shell of large curvature radius ($>1\ R_E$). In this case it is possible to evaluate its orientation and velocity with the time delay method (De Keyser et al. 2008, this issue). The velocity of the "frozen-in" material itself cannot be tracked in this way, but only that of the locally planar plasmapause surface. Figure 11 displays the four density profiles versus time in the inbound pass of 13 June 2001 (Décréau et al. 2005). Crossings of an external plasmapause knee occur between 00:00 and 00:10 UT for the trio C1–C2–C4 and about 40 minutes later for C3. The CLUSTER constellation, displayed in Fig. 2b, is elongated (largest spacecraft separation ~10 000 km), but the size of the tetrahedron formed by the four crossing positions is significantly smaller (largest distance between positions ~1000 km). The tetrahedron centre is located near 18:00 MLT and $MLAT = -35°$. Timing analysis indicates a planar boundary containing the magnetic field vectors measured onboard, as expected from a magnetic shell surface, but with an orientation (nearly facing the Sun) twisted from the expected global shape of the plasmapause. In summary, the plasmapause boundary is observed to be almost motionless during ~45 minutes. The measured orientation is compatible with the magnetic field orientation. It is, however, still somewhat questionable, as the assumption of a constant drift velocity over the total time interval is idealized.

3.4.4 Statistical Study of the Plasmapause Position and Thickness

A statistical analysis of the plasmapause position and thickness has been done with 264 CLUSTER plasmapause crossings using time-delayed values of K_p depending on the MLT of the point of measurement (Darrouzet 2006). The plasmapause has been identified by the innermost sharp density gradient, with a density drop of at least a factor of 5 over a radial distance of 1 R_E, or less. In order to facilitate inter-comparison of the CLUSTER density profiles, the parameter R_{equat} is introduced. It corresponds to the geocentric distance of the

magnetic field strength minimum along a field line, and is expressed in units of R_E (for more details see Darrouzet et al. 2004). The results are in agreement with general trend from earlier studies: For example the plasmapause forms closer to the Earth when the level of geomagnetic activity increases. It is difficult to say more, because of the limited coverage of the sample in term of MLT and K_p. Indeed, the sample contains very few plasmasphere passes corresponding to $K_p \geq 4$. This bias in the sample results from the relatively small orbital time spent by the CLUSTER spacecraft in the plasmasphere, and the rather low probability for high level of activity. Furthermore, for high K_p the plasmapause forms closer to Earth, i.e., below the perigee of CLUSTER ($\sim$4 R_E). The thickness of the plasmapause region can be determined from the equatorial density profiles. It decreases when K_p increases in all MLT sectors and has a maximum around 09:00 MLT and in the dusk sector. This result should however be taken with caution, because the database is not equally distributed in MLT (less data in the noon sector). Because of the precession of the CLUSTER orbits, the satellites cross the plasmasphere in the same MLT sector every year at the same period of the year. Therefore seasonal effect could also influence those results.

4 Ion Composition

Combining ground-based measurements with space-based remote sensing (IMAGE) and in situ measurements (CLUSTER) can capitalize on the complementary natures of these techniques. Such investigations elucidate the general question of the plasmaspheric ion composition and provide an overview of typical composition and variability.

4.1 Ion Composition from IMAGE

Dent et al. (2003) combined observations of mass densities from ground magnetometers, electron abundances from whistler measurements and from RPI, and He^+ column abundances from EUV, all taken on a geomagnetic quiet day. The shapes of radial profiles determined using these techniques were consistent with one another. Dent et al. (2003) found that, if all heavy ions are accounted for by a single species (unlikely to be true for either species they consider), the ratios by number are 35–64% for He^+ alone or 7–13% for O^+ alone for $L < 3.45$. For $L > 3.45$, their techniques suggest that relatively few heavy ions are in the outer plasmasphere. This study demonstrated also the presence of azimuthal density structures in the outer plasmasphere.

Clilverd et al. (2003) analyzed almost simultaneous determinations at $L = 2.5$ of the mass density from ground measurements of geomagnetic pulsations, the electron abundance at the same location from ducted-mode whistlers, the in situ electron abundance from RPI, and the remotely-sensed He^+ abundance from EUV. They used measurements that referred to a single geomagnetic field line and longitude, whereas Dent et al. (2003) used measurements at a specific time from different locations. Further, they include observations during two days of moderate geomagnetic disturbance. For the earlier day, Clilverd et al. (2003) inferred a He^+ abundance ratio of $\sim$3.8% by number relative to H^+ from ground magnetometer measurements. They derived a value of 3–4% for the same ratio using EUV and VLF measurements. They further noted that the L-dependence of He^+ column abundance near $L = 2.5$ has the same shape as the electron column abundance computed by integrating RPI electron measurements along EUV lines of sight. This implies that the ratio He^+/H^+ is approximately constant at this time and place, in contrast with the statistically decrease with L derived by Craven et al. (1997). The ratio He^+/H^+ is also somewhat lower than the

value of ∼10% found in Craven et al. (1997). For the second day, Clilverd et al. (2003) inferred the presence of ions heavier than He^+, and suggested O^+ as a likely candidate. By comparing the mass density and VLF-derived electron abundance, they found a ratio of 20% He^+ by number, assuming charge neutrality and a plasma whose only ions are H^+ and He^+. Although EUV gives a column abundance of He^+ higher than the first day's by a factor of 1.6, this is insufficient to account for much of the discrepancy in mass density, leading to the conclusion that heavier ions must be present.

Building on these techniques, Grew et al. (2007) used measurements of mass density from field line resonances, electron abundance from whistler measurements, and He^+ abundance from EUV, to study a 8-days interval of prolonged geomagnetic disturbance. By combining all measurements on a field line at $L = 2.5$, Grew et al. (2007) were able to solve simultaneous equations for the abundances of H^+, He^+, and heavier ions (taken to be O^+) under the assumption of charge neutrality. During their study interval, the plasmapause moved inward and outward, and also showed substantial azimuthal structure, so that the $L = 2.5$ location sampled conditions both inside and outside the plasmasphere. They found that, for most times, composition ratios were roughly similar both inside and outside the plasmasphere. For H^+:He^+:O^+, they found ∼82:15:3 by number. An interesting deviation from this norm occurred just outside the plasmasphere, when the inferred O^+ proportion reached ∼60%. This value suggests the presence of an O^+ torus consistent with the findings of Fraser et al. (2005) and the results of Clilverd et al. (2003).

4.2 Seasonal Variations

The seasonal variation has been known for some time, having been first detected in whistler measurements of the electron abundance (see, for example, the discussion in Clilverd et al. 1991). Using CRRES measurements of electron abundance, Clilverd et al. (2007) demonstrated that this variation is manifest as a maximum in equatorial electron abundance in December and a minimum in June that occurs in the longitude range of approximately −180°E to +20°E, with a maximum variation near −70°E. Outside this range of longitudes the seasonal variation is much weaker. They attribute the variation to the offset and tilt of the geomagnetic dipole, which leads to differing amounts of illumination, and hence ionization, at the foot-points of plasmaspheric flux tubes. A contributing factor is differences in thermospheric winds at high latitudes, which tend to drive the ionospheric plasma up field lines. In addition to the complete azimuthal coverage in electron abundance afforded by the CRRES measurements, Clilverd et al. (2007) included a determination of the corresponding variation in equatorial He^+ abundance. These data were extracted from summations of many EUV images acquired in June and December 2001, that is, approximately one solar cycle after the CRRES observations. The amplitude and phase of the variation in He^+ abundance match the variation in electron abundance from CRRES quite well in general, while showing some small-scale differences. Even though comparing the absolute values of the two abundances inferred from measurements of different species separated in time by a decade is of dubious value, such a comparison yields $He^+/H^+ \approx 0.25$. This value is higher than typical, yet not unreasonable.

4.3 New Methods of Studying Ion Composition in the Plasmasphere

Radio sounding in the whistler- and Z-modes by RPI onboard IMAGE led to the identification of two new methods of studying ion composition in the important altitude range between the O^+ dominated ionosphere and the H^+ dominated plasmasphere: (i) Z-mode sounding

at altitudes in the 2000–5000 km range to detect a minimum in the altitude profile of the cutoff frequency for Z-mode propagation along geomagnetic field lines. The detection of this minimum and remote sensing of its altitude can provide information on the altitude variation of ion composition. (ii) Whistler-mode sounding, primarily in a frequency range below 12 kHz, in which the variation in echo range with frequency provides information on both the distribution of total plasma density along the field line below the satellite (typically operating at 3000 km altitude) and the effective ion mass both at the satellite and along the field line between the satellite and points below ∼1000 km altitude. Those methods are outlined elsewhere in this issue (Masson et al. 2008).

4.4 Ion Composition from CLUSTER

Data provided by the CIS experiment onboard the CLUSTER spacecraft, when operating in the Retarding Potential Analyzer (RPA) mode, allow accurate measurements of the ion distribution functions and composition in the approximate energy range 0.7–25 eV/q (with respect to the spacecraft potential), covering the plasmasphere energy domain. Figure 12 displays a typical ion mass spectrum, obtained by CIS during a plasmasphere pass in the nightside sector, close to the magnetic equator, on 18 March 2002. The magnetospheric conditions during this event were quiet ($K_p = 1^+$). The characteristic peaks of H^+ and He^+ are clearly present. He^{++}, if present, would be almost "washed-out" by the tail of the H^+ distribution (spillover). The height of the H^+ peak is not proportional to the relative abundance, because a different sampling law was used for the other ion species (sampling law change at channel 26). Figure 12 indicates no O^+ ions above the measurement background. The small background present over all time-of-flight channels is due to penetrating particles from the radiation belts.

Dandouras et al. (2005) studied a plume crossing on 31 October 2001 in the morning sector (08:45 MLT), during quiet magnetospheric conditions. The plume was observed after exit from the main plasmasphere, in the outbound leg of the orbit. No background is present, and the spectrum exhibits the characteristic peaks of H^+ and He^+. It also shows the absence of O^+ ions, at a significant level. An upper limit of about 0.04 cm^{-3} for the O^+ density in the plume has been estimated. This value has to be compared to 0.8 cm^{-3} for the H^+ density and 0.14 cm^{-3} for the He^+ density. Note that these are partial density values, in the energy range covered by CIS in RPA mode.

Dandouras et al. (2005) performed a systematic survey with CIS data to search for low-energy O^+ ions, during the period July 2001–March 2003. Those observations are outside

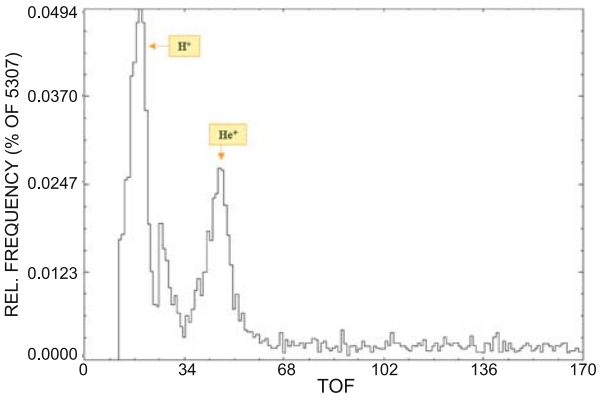

Fig. 12 Time-of-flight spectrum for the ions detected by CIS onboard C3 on 18 March 2002 between 10:40 and 10:50 UT. The *abscissa axis* is the time-of-flight channel number (inversely proportional to the ion velocity) and the *ordinate axis* is the number of particles in a given channel, with two different sampling laws above and below channel 26

the main plasmasphere, and most of them correspond to upwelling ions, escaping from the ionosphere along high-latitude magnetic field lines. For few of these events, the O^+ distributions are bi-directional and indicate detached plasma, originating from deeper in the plasmasphere and having an outward expansion velocity towards higher L-shell. For example, C4 observed on 2 October 2001 in the morning sector (09:45 MLT, $L \approx 6$) detached plasma, including O^+ ions, with symmetric bi-directional distributions and an outward expansion velocity of ~ 3 km s^{-1}. Note, however, that O^+ ions were never observed in the main plasmasphere, above instrument background, at CLUSTER altitudes (perigee $\sim 4\ R_E$).

4.5 Average Ion Mass from Alfvén Waves

Additional information about ion composition can be determined from the frequencies of toroidal (azimuthally oscillating) Alfvén waves observed in space (Denton 2006) or on the ground (Waters et al. 2006). From the frequencies of observed Alfvén waves, the total mass density ρ_M can be determined from a solution of the wave equation (Denton 2006). If the electron density n_e is independently available, like from plasma wave measurements (LeDocq et al. 1994), the average ion mass M can be determined. Assuming that the plasma consists predominantly of H^+, He^+ and O^+, M is:

$$M \equiv \frac{\rho_M}{n_e} \simeq 1 + 3\frac{n_{He^+}}{n_e} + 15\frac{n_{O^+}}{n_e}. \tag{1}$$

Equation (1) provides a constraint on the relative He^+ and O^+ densities. Furthermore, there are indications that the He^+ density is not nearly as sensitive to geomagnetic activity as is that of O^+ (Craven et al. 1997; Krall et al. 2007). This suggests that if M is significantly greater than unity, n_{O^+}/n_e is approximately equal to $(M-1)/15$.

Recently, Denton et al. (2008) used Alfvén frequencies measured by CLUSTER to determine ρ_M with unprecedented accuracy for two events at perigee ($L = 4.8$). By combining the values of ρ_M with n_e determined by the WHISPER instrument, Denton et al. (2008) found $M = 4.7$ when $n_e = 8$ cm^{-3} (28 October 2002, 02:33 UT), and $M = 2.9$ when $n_e = 22$ cm^{-3} (10 September 2002, 12:07 UT). These values imply approximate relative O^+ concentrations of 25% and 13%, respectively. Note that both cases are for the low densities characteristic of the plasmatrough. The CIS instrument was also used to determine the O^+ ring current density, but was limited to particle energies >40 eV, because CIS was not operating in the RPA mode at these orbits. The amount of O^+ measured by CIS was not negligible, but was still not nearly enough to account for the inferred ρ_M. This indicates that the bulk of the O^+ density is cold particles that are not measured by CIS, when not operating in the RPA mode. For the 10 September 2002 event, Denton et al. (2008) used the four CLUSTER spacecraft to infer the distribution of electron density. They assumed a model distribution and adjusted the parameters of the model to minimize the difference between the observed and modeled density. Figure 13 displays ρ_M and n_e for the 10 September 2002 event, along with H^+ and O^+ densities assuming a H^+/O^+ plasma. The results suggest that there is a trapped equatorial distribution of O^+.

5 Plasmaspheric Plumes

The plasmasphere often exhibits a feature that extends beyond the main plasmapause towards the dayside magnetopause (e.g., Moldwin et al. 2004). This feature, named the plasmaspheric plume, has been routinely observed by the EUV imager onboard IMAGE, but also

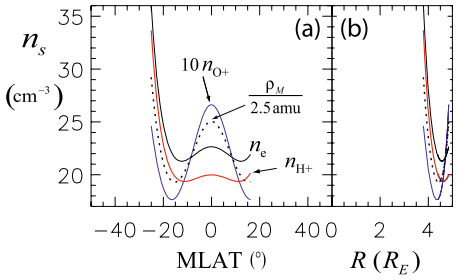

Fig. 13 Field line distribution of species s density n_s versus **a** magnetic latitude *MLAT* and **b** geocentric radius R on 10 September 2002. The *solid black curve* is the electron density n_e found using the four CLUSTER spacecraft, the *dotted black curve* is the mass density ρ_M divided by 2.5 amu based on Alfvén frequencies measured by C1. The *red* and *blue solid curves* are the H^+ and O^+ densities consistent with n_e and ρ_M assuming a H^+/O^+ plasma (the O^+ density has been multiplied by 10). (Adapted from Denton et al. 2008)

by the four CLUSTER spacecraft or both. Plasmaspheric plume signatures have also been detected in the ionosphere, in particular with measurements of the total electron content (TEC) by global positioning system (GPS) satellites. The combination of those different dataset facilitates a great deal of progress in understanding the genesis and evolution of plumes in response to ever-changing levels of geomagnetic activity.

5.1 Overall Plume Formation

Global images obtained by EUV onboard IMAGE revolutionized the community's system-level picture of the plasmaspheric response to storms and substorms. EUV images demonstrate conclusively that plumes form in a series of phases that are directly driven by geomagnetic conditions. Figure 14 illustrates those phases during the plasmaspheric erosion event on 18 June 2001. During quiet conditions, the plasmasphere expands in size in response to filling of flux tubes with ionospheric plasma (Fig. 14a). A strong negative solar wind electric field (shown on Fig. 14m), corresponding to strong geomagnetic activity, initiated a sunward surge of plasmaspheric plasma (Figs. 14b–d): The nightside plasmapause moves inward, and the dayside moves outward to form a broad, sunward-pointing plume. Under the influence of continued high activity the dayside plume maintains its sunward orientation but becomes progressively narrower in LT (Figs. 14e–h). Finally, the waning of geomagnetic activity relaxes the plume's sunward orientation, and the plume begins rotating eastward with the rest of the plasmasphere and Earth (Figs. 14i–l). These phases (sunward surge, plume narrowing, plume rotating) are a consistent part of the plasmasphere's response to changes in geomagnetic activity, as confirmed in numerous studies using EUV data, either alone or in combination with in situ measurements (Sandel et al. 2001, 2003; Goldstein et al. 2003a, 2004b, 2005b; Goldstein and Sandel 2005; Spasojević et al. 2003, 2004; Abe et al. 2006; Kim et al. 2007). These global observations of plasmaspheric phases provide context for many in situ plume studies that have been performed (Garcia et al. 2003; Chen and Moore 2006; Darrouzet et al. 2006a; Borovsky and Denton 2008; Darrouzet et al. 2008). A brief discussion of plasmaspheric phases, in the context of physics-based models, is contained elsewhere in this issue (Pierrard et al. 2008).

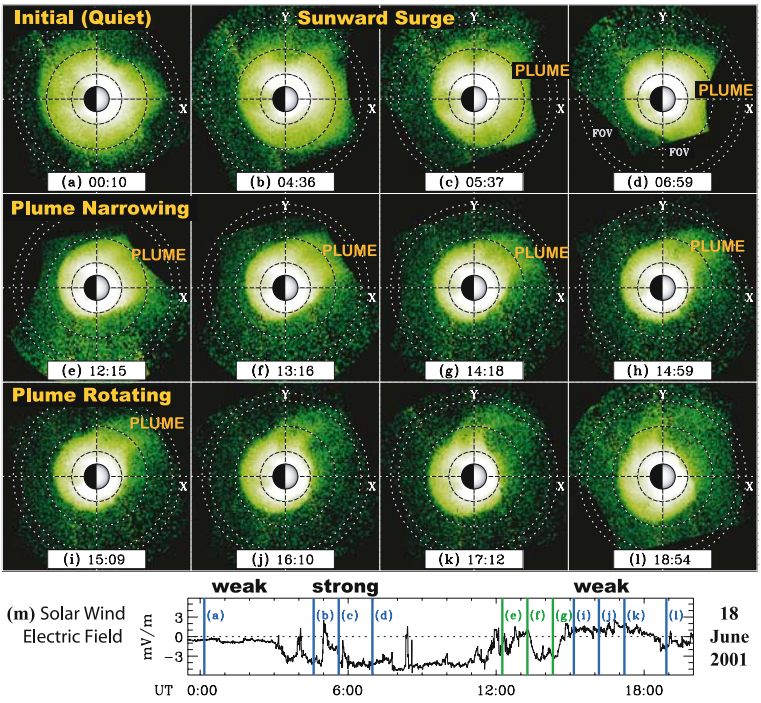

Fig. 14 **a**–**l** Plasmasphere EUV images, mapped to the magnetic equatorial plane (in SM coordinates), with the Sun to the right and *dashed circles* at $L = (2, 4, 6, 6.6)$. The field of view (FOV) edges are indicated in panel **d**. **m** Dawnward solar wind electric field (in geocentric solar magnetospheric, GSM, coordinates), defined as the product between the solar wind speed and the IMF B_Z, so that this electric field is negative when the IMF is southward. (Adapted from Goldstein and Sandel 2005)

5.2 Plume Structure and Evolution on Large Scales

5.2.1 Complicated Structure

The CLUSTER mission phase at 5000 km spacecraft separation corresponds to orbit planes exploring the plasmasphere in different LT sectors, at respectively the inbound part of the orbit (southern hemisphere, later LT) and its outbound part (northern hemisphere, earlier LT). Figure 15 displays WHISPER observations in such a case, as well as boundary positions derived from their analysis. The event chosen here, on 5 July 2002, occurs at the end of a period of slightly increasing disturbance (K_p from 1^+ to 4). Several large-scale features are clearly seen on the WHISPER electric field spectrograms (Fig. 15a): (i) the plasmasphere body at the centre of each plot (20:45–22:10 UT for C4); (ii) a plume in the southern hemisphere (20:00–20:30 UT for C4); (iii) a plume in the northern hemisphere (22:30–22:45 UT for C4). Spectrograms for the other spacecraft display similar features, at different times.

Arrows, pointing towards plumes, delimit the time intervals covering the low density channel between each plume and the plasmasphere (see Sect. 7). The positions of satellites at each side of an arrow can be projected along field lines in the equatorial plane, providing the 2-D view displayed in Fig. 15c, where possible motions of the low density channels are ignored, i.e., as if all boundary crossings occurred simultaneously. Several interesting spatio-temporal aspects can be learned by analysing Fig. 15a, which provides the chronology of

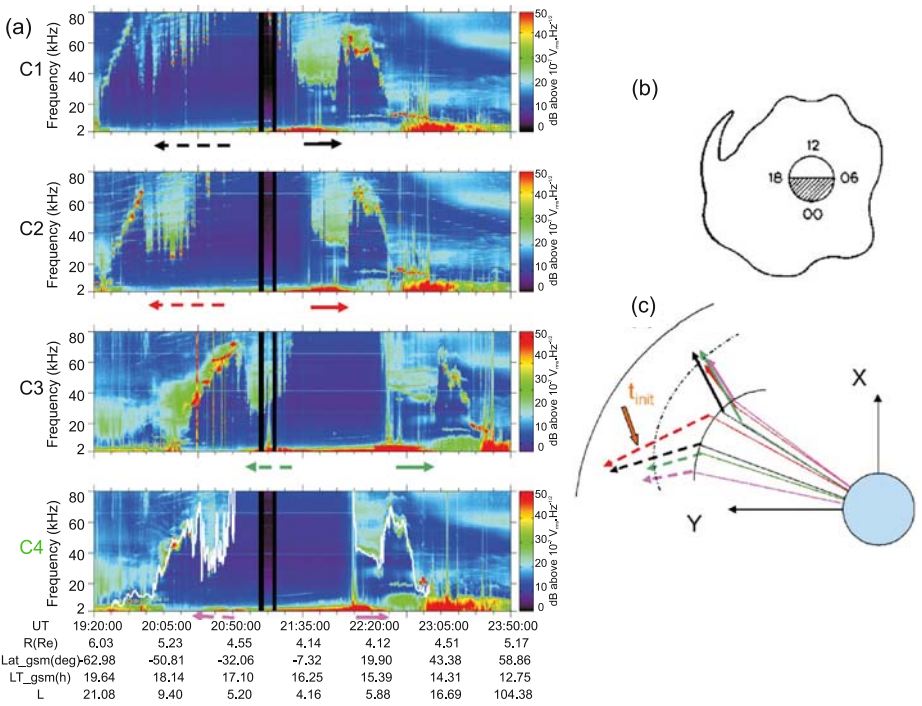

Fig. 15 **a** Frequency–time electric field spectrograms from WHISPER onboard CLUSTER displaying a plume structure observed on 5 July 2002 in both hemispheres. The evolution of the plasma frequency during a pass is plotted in white for C4. The *arrows* (*dashed* in the southern hemisphere and *solid* in the northern hemisphere), pointing towards the plume, delimit time intervals covering the low density channel between the plume and the plasmasphere. **b** Sketch of a type of spatial irregularity in the equatorial cross-section of the plasmasphere expected during a period of increasing disturbance. (Adapted from Carpenter 1983.) **c** Positions of low density channels observed by the four CLUSTER spacecraft plotted in the equatorial cross-section of the plasmasphere in GSM coordinates

observations, and Fig. 2a, which provides the shape of the constellation: The spacecraft order along the orbit is C1, C2, C4 and C3, and the order in increasing LT is C1, C2, C3 and C4. The feet of the arrows, indicating the plasmapause boundary, are crudely aligned with a quasi-cylindrical shape, except for the C3 northern crossing, which is inward from the others. This could be due to a slight undulation of the plasmapause, as illustrated in Fig. 15b.

The view of Fig. 15c could be modified, in order to take account of large-scale drifts of frozen-in material. The main drift that could be taken account of is corotation (Darrouzet et al. 2008). Out of the eight plasmapause crossings, two of them occur at the same time (∼21:30 UT): outbound of C1 (foot of the black solid arrow) and inbound of C3 (foot of the green dashed arrow). It is possible to draw a picture at that common time of reference, by assuming that all frozen-in field lines are corotating. In such a picture, the solid arrows would be displaced and rotated westward, up to ∼20°, still placed inside the indicated channel feature. The dashed arrows would be displaced eastward similar amounts. It is clear that corotation is not likely to be a valid assumption at the beginning of the analyzed period. Indeed, the density profiles inside the channels show a striking evolution from the first crossing (C1, inbound), to the last one (C3, outbound). The event can be split in two successive

phases. During the initial hour (19:40–20:40 UT) the low density channel is not well formed, but filled up by a large number of dense, narrow, plumes. C1, located at an earlier LT than C2, sees more material than C2, at roughly the same UT time. The time and space evolution of those blobs is unclear. No one-to-one correlation of density blobs seen respectively on C1 and C2 is apparent. Data from EDI and EFW onboard CLUSTER indicate fluctuations of large-scale electric field at the same time period. The small size plumes progressively disappear (see C2, C4 inbound). During the last part of the crossing (20:50–23:00 UT), the channel structure is well established, cleaned up from small size plumes. It is likely that, during that time period, the assumption of corotation is valid. It is not during the first part.

5.2.2 Global Visualisation of a Plume Crossing

Darrouzet et al. (2008) studied a CLUSTER plasmasphere pass characterized by a very large spacecraft separation (10 000 km). This event on 18 July 2005 between 13:00 and 20:00 UT, is located around 15:00–16:00 MLT, with a maximum value of K_p in the previous 24 hours equal to 5^+. Plume crossings are seen during the inbound pass in the southern hemisphere (SH), and also during the outbound pass in the northern hemisphere (NH). Lots of differences are seen in terms of the L position of the plume between the four spacecraft. This is logical, as some of the satellites cross the density structure a few hours after the first one; during this time period, the plume rotated around the Earth and moved to higher L values. The inner boundary of the SH plume is seen around $L = 7.0$ by C1, whereas this boundary is crossed 2 hours later by C3 and C4 around $L = 8.3$. Knowing that the MLT position of the plume crossing is quite similar for those three satellites, one can then calculate an average radial velocity of the plume at fixed MLT of the order of 1.2 km s^{-1}, which is consistent with the results by Darrouzet et al. (2006a). For this event, around 15:00–16:00 MLT, this corresponds to a Sunward motion.

The L-width ΔL of the plume is very different between the spacecraft, and also between the inbound and outbound crossings for some satellites. For C1, $\Delta L = 3.2\ R_E$ during the inbound pass in the SH, and 2.6 R_E during the outbound pass in the NH. This means that the outbound crossing, taking place a few hours after the inbound one, detects a narrower plume. There is a similar trend for the other satellites. Except for C2, the maximum electron density inside the plume is always higher in the inbound pass than in the outbound one. All those characteristics can be explained by plume rotation so that the outbound crossings occur at greater distance along the plume, where the plume is narrower and has lower density.

More information can be deduced if CLUSTER trajectories are projected along magnetic field lines onto the equatorial plane. As the spacecraft separation is quite large and in order to be able to compare the four trajectories and the eight crossings, one can assume that the plasmasphere and its sub-structures are in corotation with the Earth. Figure 16 presents such a projection in a corotating GSM frame of reference. The plasmapause is clearly seen on the trajectories of C1 and C2 at a radial distance of $\sim 5\ R_E$, where the color coded density changes from green to yellow. A clear plasmapause is not crossed by C3 and C4. This could be because the plasmasphere is located closer to the Earth at the LT position and UT time of C3 and C4. The inbound plume crossings by the four satellites, and the outbound crossings by C1 and C2, are clearly crossings of the same plume, which corotates as time elapses between successive crossings. The outbound crossing by C3 and C4 (bottom right of Fig. 16) is probably another density structure and/or the effect of strong time variations.

A few other studies analysed plasmaspheric plumes at large-scale with CIS (Dandouras et al. 2005) and WHISPER (Darrouzet et al. 2004; Décréau et al. 2004).

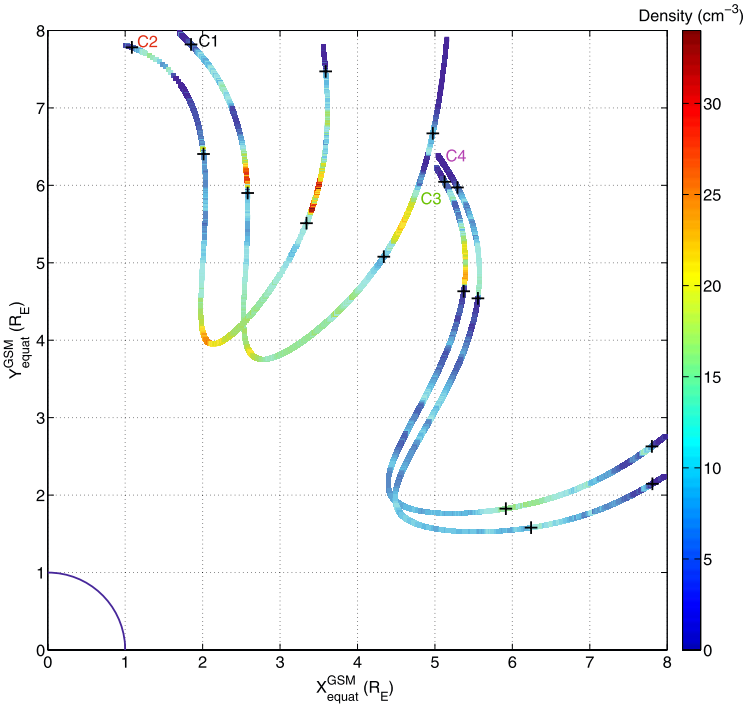

Fig. 16 Electron density plotted along the trajectories of the CLUSTER satellites and projected along magnetic field lines onto the equatorial plane in a corotating GSM frame of reference (chosen such that C4 was at 15:30 MLT at 18:00 UT), during the plasmasphere pass on 18 July 2005. The density is plotted with the color scale on the *right*. The plasmasphere passes start at the label of each satellite (on the *left*), and end on the *right* side. The *crosses* give the times of the plume crossings computed from the spectrograms. (Adapted from Darrouzet et al. 2008)

5.3 Plume Structures on Small Scales

Darrouzet et al. (2006a) studied three plume crossings by CLUSTER at times of small spacecraft separation, for which multipoint analysis tools can be used. One of the events is on 2 June 2002, between 12:00 and 14:30 UT, in the dusk sector (18:00 MLT) and with moderate geomagnetic activity. A very wide plume is seen in SH and NH on all four spacecraft. The electron density profiles of the plume as determined from WHISPER and EFW (for the part above 80 cm^{-3}) are displayed in Fig. 17. Both structures have the same overall shape. This indicates that these are crossings of the same plume at southern and northern latitudes of the plasmasphere. This also suggests that the plume did not move much over the 2 hours between both plume crossings. To confirm this global statement, one can compute the equatorial normal velocity of the plume boundaries V_{N-eq}, by using the time delay method described elsewhere in this issue (De Keyser et al. 2008). Those velocities, given on the figure for several plume boundaries, are quite small for the inbound plume crossing (larger at the outer edge than at the inner one). From those boundary normal velocities, Darrouzet et al. (2006a) derived an azimuthal plasma velocity V_{P-eq}. They found that for the outer boundary of the inbound crossing, $V_{P-eq} = 6.9 \pm 1.2$ km s^{-1}, which is much higher than the corotation velocity (between 3.6 and 2.8 km s^{-1} at these spacecraft

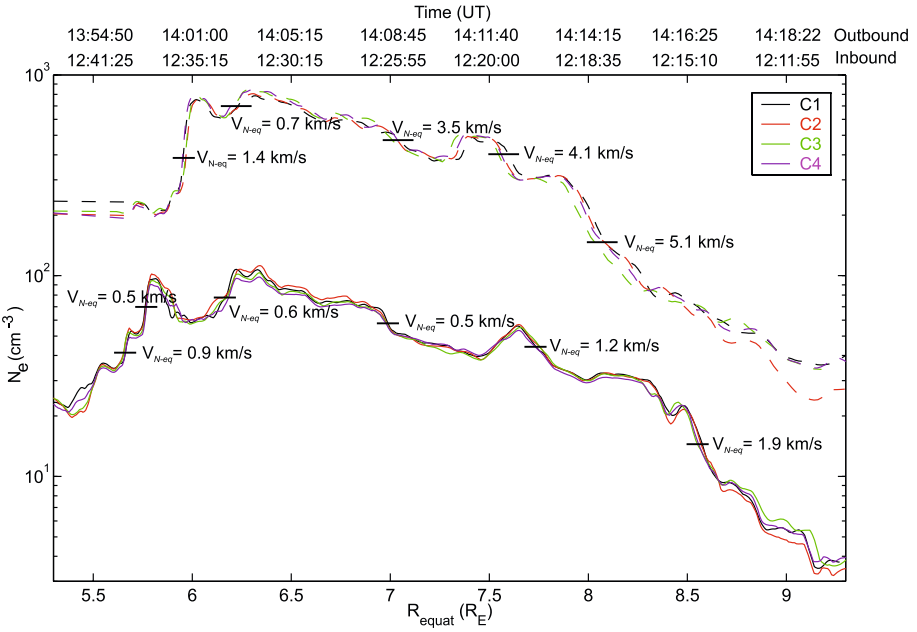

Fig. 17 Electron density profiles as a function of R_{equat} for the two plume crossings by the four CLUSTER satellites on 2 June 2002. The *lower curves* correspond to the inbound pass and the *upper curves* (shifted by a factor 10) to the outbound pass. The magnitude of the normal boundary velocity V_{N-eq} derived from the time delay method and projected onto the magnetic equatorial plane is indicated on the figure. (Adapted from Darrouzet et al. 2006a)

positions). This could also be compatible with a lower azimuthal speed if there is an outward plasma motion as well. The velocity is also higher than the corotation velocity at the inner edge, $V_{P-eq} = 4.0 \pm 1.2$ km s^{-1}. For the outbound crossing, there are also deviations from corotation. By computing the average radial velocity of the plume edges, Darrouzet et al. (2006a) demonstrated that the plume is thinner in the NH pass than in the SH pass, and that its inner edge is at a larger equatorial distance. They prove also that the instantaneous measurements are in agreement with long term motion of the plume. EDI measures a drift velocity of the order of the corotation velocity, mainly in the azimuthal direction but with a radial expansion of the plume.

To check those results, it is very useful to combine in situ data with global data from IMAGE. On an EUV image taken at 12:33 UT (close to the time of the inbound plume crossing by CLUSTER), a very large plume is observed in the post-dusk sector, with its foot attached to the plasmasphere between 17:30 and 22:00 MLT (Darrouzet et al. 2006a). This is consistent with the WHISPER observations. As the plume is observed on EUV images during several hours, the motion of the plume can be determined. The foot of the plume (at 3.7 R_E) moves at a velocity of 1.6 ± 0.1 km s^{-1}, close to the corotation velocity 1.7 km s^{-1}. The extended part of the plume is clearly moving slower than the foot and away from the Earth.

LANL geosynchronous satellites confirm the presence of the plume: LANL 97A observes a large density structure as it orbits Earth from 12:00 to 22:00 MLT. This is consistent with the plume seen by IMAGE between 17:30 and 22:00 MLT and observed by CLUSTER at 12:30 UT and at $R_{\text{equat}} = 6.5\ R_E$.

5.4 Statistical Analysis of Plasmaspheric Plumes

Darrouzet et al. (2008) performed a statistical analysis of plasmaspheric plumes with a very large CLUSTER database starting in February 2001 and covering exactly five years, to ensure equal coverage of all MLT sectors. Due to the polar orbit of CLUSTER, the spacecraft usually cross the plumes only at great distance from the foot attached to the plasmasphere. The dataset contains 5222 plasmasphere passes with data (85% of the total number of passes) and offers global coverage of all MLT sectors, above $L = 4$ (perigee of CLUSTER). 782 plume crossings have been observed, which corresponds to 15% of the plasmasphere passes with data. More plumes are found at low and middle L values (5–8 R_E), in the afternoon and pre-midnight MLT sectors (see Fig. 18). Some plumes are observed at high L, especially in the afternoon MLT sector and there are very few plumes in the post-midnight and morning MLT sectors.

The dataset used by Darrouzet et al. (2008) contains passes for almost all K_p values, but mostly for low to moderate geomagnetic activity. There are only a few plasmasphere passes with high activity, mainly because the plasmasphere is closer to the Earth in this case, and therefore not crossed by the CLUSTER satellites. No plumes are observed for the highest K_p, the highest *am* and the lowest *Dst*. In such case the plasmasphere moves closer to the Earth, sometimes below the perigee of CLUSTER (4 R_E), and if there would be a plume, it would be difficult to unambiguously identify it (because of the absence of a crossing of the main plasmasphere). In such case, CLUSTER could also miss a plume because it narrows quickly in MLT during times of high activity and the spacecraft have to pass through perigee in the appropriate MLT to see it.

Plumes are found to have all possible density variations in the range accessible to WHISPER (up to 80 cm^{-3}), but with more events with small density variations (<30 cm^{-3}). Plumes do not appear to have a preferred maximum density value. There are more plume crossings with a short time duration. The L-width ΔL of the plumes varies up to 6 R_E, but with more events at smaller values (the characteristic value is 1.2 R_E). The broadest plumes are observed in the afternoon MLT sector and at high L, while the narrowest ones are seen at small L (<7 R_E) and mostly in the afternoon and pre-midnight MLT sectors. Less dense

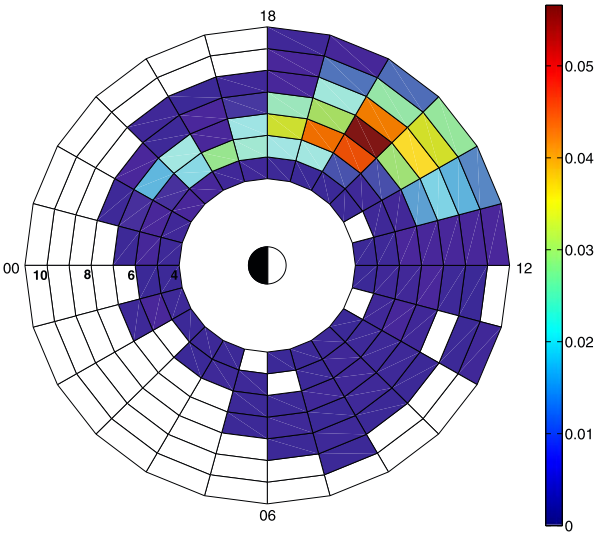

Fig. 18 Probability of being inside a plume for each [L,MLT] bin, normalized by the distribution of all the trajectories. L varies between 4 and 11 R_E. (From Darrouzet et al. 2008)

plumes are observed at all L distances (mostly >7 R_E) and mainly in the afternoon MLT sector. Denser plumes (>40 cm^{-3}) are observed especially at small L (5–7 R_E) and in all MLT sectors (except morning), although mostly in the afternoon and pre-midnight MLT sectors.

Pairs of plume crossings, during the inbound and outbound plasmasphere passes, make it possible to examine the transformation of a plume on a time scale of a few hours and the corresponding change in LT. Darrouzet et al. (2008) computed the apparent radial velocity of the inner boundary of a plume crossed in both hemispheres, assuming that both crossings are observed approximately at the same MLT. This velocity ranges between -1.5 and $+1.5$ km s^{-1}, due to the large diversity of the plume database, but with values mostly positive, which shows an apparent outward motion of the plume towards higher L values. The mean apparent radial velocity is around 0.25 km s^{-1}, in agreement with a previous study by Darrouzet et al. (2006a).

5.5 The Plasmasphere–Ionosphere Connection

In the last few years, the importance of plasmaspheric plumes in magnetospheric dynamics has been emphasized with simultaneous observations of ring current and cold plasmaspheric plasma by IMAGE, and with global ionospheric maps from GPS-derived TEC data. These observations indicate that plasmaspheric plumes play a crucial role in mid-latitude ionospheric density enhancements (Foster et al. 2002; Yizengaw et al. 2006), polar ionization patches (Su et al. 2001) and are strongly correlated with the loss of ring current ions (Burch et al. 2001b; Brandt et al. 2002; Mishin and Burke 2005). Plumes are also associated with enhanced wave growth that can lead to pitch-angle scattering and energization of particles (e.g., Spasojević et al. 2004).

Foster et al. (2002) showed that storm-time density enhancements observed in TEC and incoherent radar studies map to plasmaspheric plumes, which are observed with unprecedented detail with EUV. Figure 19 presents an example of a mid-latitude ionospheric density enhancement observed with GPS receivers over North America, and its comparison with the plasmapause location as determined by EUV. During strong storms, a long-lived region of

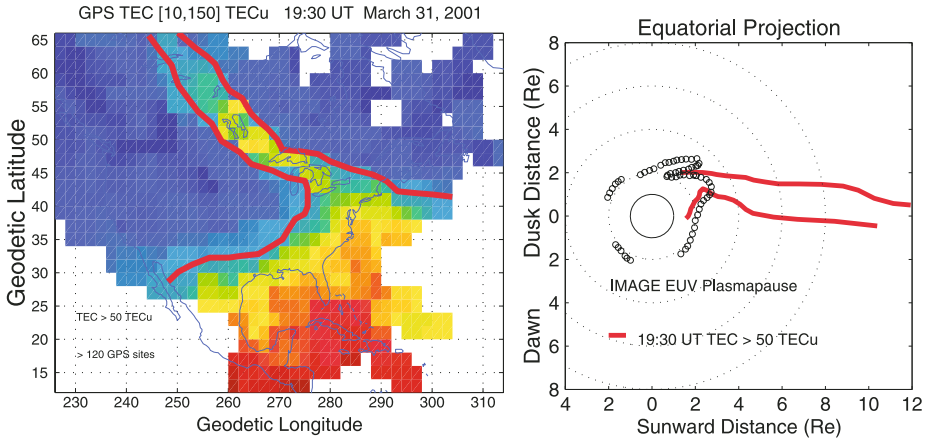

Fig. 19 (*Left*) A ground-based GPS TEC observation of a mid-latitude ionospheric plume. (*Right*) The plume extent mapped to the corresponding EUV deduced plasmapause. The *red lines* map the contour of >50 TECu. (Adapted from Foster et al. 2002)

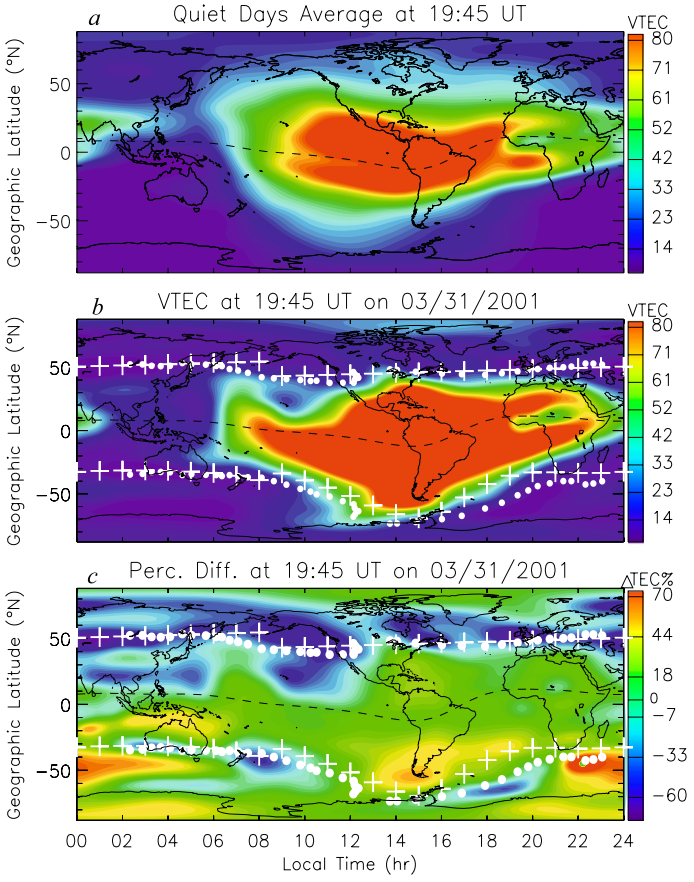

Fig. 20 15-minutes average global contour maps of GPS TEC: **a** six quiet days average, **b** data on 31 March 2001 and **c** percentage difference between data on panels **a** and **b**. The *white dots* and *plus sign* in panels **b** and **c**, respectively, depict the plasmapause locations extracted from EUV and the empirical positions of the mid-latitude trough. (Adapted from Yizengaw et al. 2005)

elevated TEC forms in the vicinity of Florida near dusk at the foot of the erosion plume and persists into the night sector. Foster et al. (2005) combined ground-based and in situ observations in the topside ionosphere, to suggest that this enhancement results from a poleward redistribution of low-latitude ionospheric plasma during the early stages of a strong geomagnetic disturbance. Simultaneous EUV observations of the plasmasphere co-locate the low-latitude TEC enhancement with a brightening and apparent bulge in the inner plasmasphere. The enhanced features, seen both from the ground and from space, corotated with the Earth once they were formed. These effects are especially pronounced over the Americas and Foster et al. (2005) suggested that this results from a strengthening of the equatorial ion fountain due to electric fields in the vicinity of the South Atlantic Anomaly.

Yizengaw et al. (2008) demonstrated that EUV observes plumes at all longitudes, but that TEC signatures of plumes are more common in the North American sector, though weaker plume signatures are seen over Europe and Asia. This study and many earlier demonstrate that plumes are most often observed in the aftermath of enhanced geomagnetic activity (not just geomagnetic storms as defined by some minimum *Dst* value) and that they tend to ap-

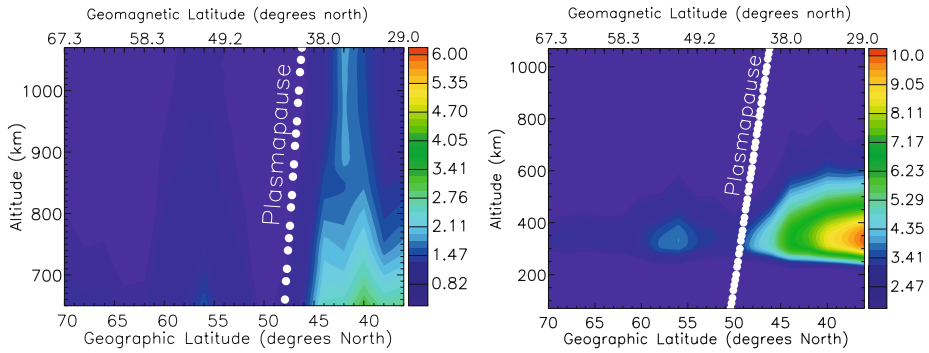

Fig. 21 Tomographically reconstructed electron density of (*left*) topside and (*right*) F-layer ionosphere, performed on 31 March 2001 using multi-direction ground-based GPS TEC from meridionally (at 16°E geographic) aligned GPS receivers. The *vertical white dots* are plasmapause positions as determined from EUV. (Adapted from Yizengaw and Moldwin 2005)

pear at earlier LT with an increase of geomagnetic activity. Garcia et al. (2003) demonstrated that the plume density enhancement exists at high geomagnetic latitude, by combining RPI wave data and EUV plume images.

In addition to plumes, ionospheric electron density exhibits complicated latitudinal structure mainly during periods of increased solar activity. The associated disturbances often result in large TEC gradients. Figure 20a displays global TEC maps showing an average quiet day distribution. The main features include the day-night asymmetry and the latitudinal structure of the low and mid-latitude ionosphere including the clear Appleton anomalies in the afternoon/dusk sector. Figure 20b displays the TEC behaviour during enhanced geomagnetic activity and Fig. 20c is a difference plot of the disturbed time compared to the average quiet time. There is a close correspondence of the mid-latitude trough and the ionospheric projection of the plasmasphere. The plume, especially in the northern hemisphere, is clearly identified in these TEC maps.

Recently, tomography has been used to establish that the altitude extent and structure of the topside ionosphere at the equatorward-edge of the ionospheric trough maps along the inferred location of the plasmapause as determined from EUV (Yizengaw and Moldwin 2005). Figure 21 presents results of the comparison of tomographic reconstruction of topside (left panel) and F-region ionosphere (right panel) during a geomagnetic storm, with the mapped location of the plasmapause as determined from EUV. The close correspondence of the mid-latitude trough and plasmasphere demonstrates the power of GPS tomography in tracking the magnetospheric-ionospheric coupling.

6 Notches

One of the recently named plasmaspheric density structures identified by EUV are notches. It is one of the largest density structures in the plasmasphere after the plume. Notches are also observed by CLUSTER but are often difficult to distinguish from other types of density structure. The observation of the evolution of notches reveals departures from corotation in the plasmasphere.

6.1 Observations of Notches

Notches are characterized by deep, mostly radial density depletions in the outer plasmasphere that can extend inward to $L = 2$ or less (Sandel et al. 2000; Gallagher et al. 2005). The MLT-width ranges from ∼0.1 to ∼3 hours MLT and the notch shape can be maintained for several days as it refills with ionospheric plasma. Notches are likely included among the features previously referred to as density cavities inside the outer plasmasphere (Carpenter et al. 2002). Figure 22 illustrates a plasmaspheric notch seen by EUV on 31 May 2000. In this case the notch is a broad density cavity at dusk. Notches sometimes include a central prominence of enhanced plasma density.

Notches have also been observed by CLUSTER, in particular with the WHISPER instruments. It can be seen as a decrease of the density inside the plasmasphere. However, it is often difficult to distinguish from a plume or another structure. When available, this can be resolved with global images of the plasmasphere from EUV onboard IMAGE. Figure 23 presents a notch crossing observed by WHISPER onboard C4 on 9 July 2001. Notches are very often associated with both continuum radiation features over the high end of the WHISPER frequency range, and intense electrostatic emissions thought to be primary sources of

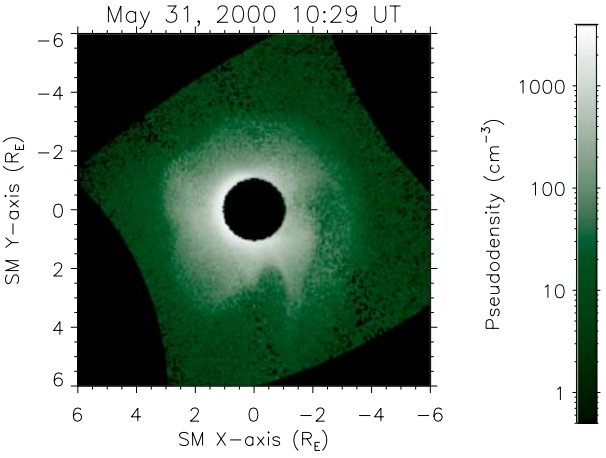

Fig. 22 Pseudodensity image from EUV taken onboard IMAGE at 10:27 UT on 31 May 2000 and projected in the SM equatorial plane. A plasmaspheric notch is observed in the dusk side

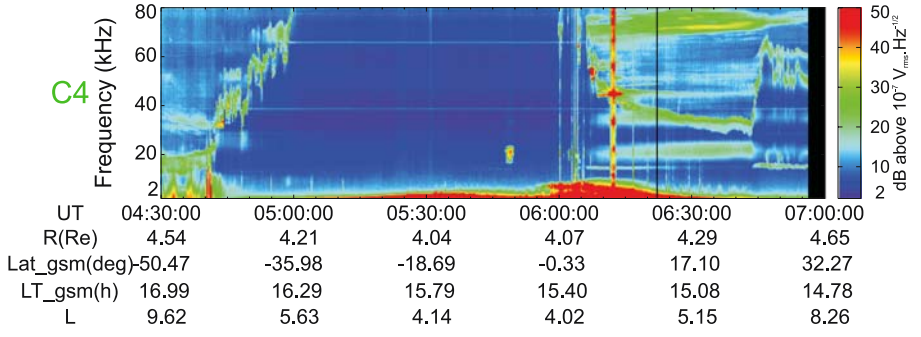

Fig. 23 Time–frequency electric field spectrogram measured by WHISPER onboard one CLUSTER spacecraft, C4, during a plasmasphere pass on 9 July 2001. The magnetic equator is crossed around 05:45 UT, and a notch between 06:05 and 06:45 UT. Continuum radiations are observed during this time interval between 65 and 80 kHz. (Adapted from Décréau et al. 2004)

continuum (Décréau et al. 2004). Using IMAGE data, Green et al. (2004) demonstrated that a notch structure is typically a critical condition for the generation of kilometric continuum radiation, but that notches do not always provide the conditions necessary for the generation of the emission. More details on waves related to notches can be found elsewhere in this issue (Masson et al. 2008).

6.2 Departures from Corotation

Sandel et al. (2003) reported the first evidence that the cold plasma comprising the main body of the plasmasphere does not always corotate with Earth. They tracked notches, persistent distinctive lower-density regions seen in EUV images of the plasmasphere, to infer the motion of particular volume elements of plasma. They defined the parameter ξ, which is the ratio of the observed angular rate to the angular rate of Earth's rotation. Thus $\xi = 1$ for corotating plasma. For $\xi < 1$, the plasma lags corotation, and therefore moves westward relative to Earth, and for $\xi > 1$, the plasma moves eastward relative to Earth.

The thirteen episodes used in this initial study by Sandel et al. (2003) had durations of 15 to 60 hours; the average duration was 31 hours. The average value of ξ was 0.88, and ξ ranged between minimum and maximum values of 0.77 and 0.93 when averaged over the full duration of the episode. During some of the intervals, the westward drift rate was uniform (ξ was constant) but in other cases the drift rate varied and in some episodes and times during the interval of observation, ξ was near 1. Figure 24 illustrates an example of a long-lasting notch that was used to determine ξ. Over the 60 hours that it was distinguishable from background plasma, the notch initially seen at about 07:30 MLT in Fig. 24b moved at a nearly constant rate of $\xi \approx 0.90$. Notches of large radial extent sometimes maintained their shape for many hours, implying that at these times shearing motions, such as might be expected to arise from any L-dependent variations in ξ, were absent.

Burch et al. (2004) argued that departures from corotation in the plasmasphere are driven by corresponding motions of plasma in the ionosphere, where departures from corotation are often observed. In a study of one of the episodes of sub-corotation reported by Sandel et al. (2003), they compared DMSP measurements of ionospheric ion drifts to the motion of a notch in the plasmasphere observed by EUV at the same time. The ion drift measurements came from the same longitude range as the notch, and from latitudes corresponding to the position of the notch in L. Over the 60 hours of the episode, the motion of the notch in the plasmasphere was consistent with that expected on the basis of the azimuthal

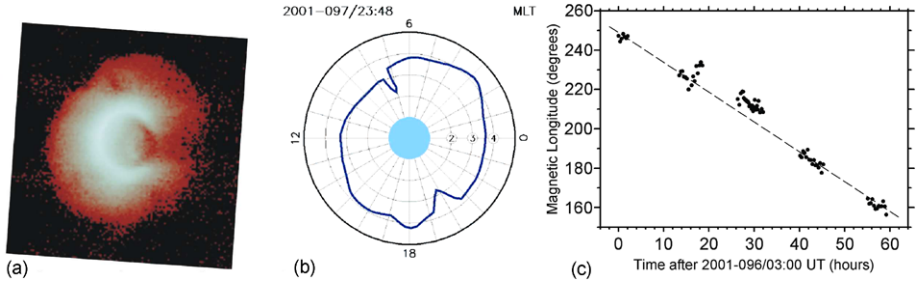

Fig. 24 **a** EUV image at 23:48 UT on 7 April 2001, illustrating two notches separated by ∼180° in azimuth. **b** Mapping of prominent brightness gradients to the plane of the magnetic equator in [L,MLT] space. **c** Magnetic longitude of the notch observed near 07:30 MLT in panel **b** as a function of time; the *dashed line* corresponds to an angular velocity that is 90% of the corotation velocity. (Adapted from Sandel et al. 2003)

ionospheric drifts if the two populations moved together, i.e., assuming that the MHD approximation applies. Burch et al. (2004) suggested that ionospheric corotation lag arises from the ionospheric disturbance dynamo (Blanc and Richmond 1980). Heating of the auroral ionosphere by currents and precipitating particles drives transport towards the equator. As the winds move to lower latitudes, conservation of angular momentum leads to a departure from corotation that takes the form of a westward drift.

A recent study by Galvan et al. (2008) found that the plasmasphere on average subcorotates at 85% of corotation, with intervals of both sub-corotation and super-corotation. Gallagher et al. (2005) studied the azimuthal motion of 18 notches seen in EUV images. For most of the notches, they derived values of ξ in the range of 0.85 to 0.97. They report one instance of $\xi = 1$, and two much smaller values of $\xi = 0.44$ and 0.74. For 12 of the 18 observations, Gallagher et al. (2005) found that DMSP Ion Drift Meter measurements were available at the relevant locations and times, and they used these measurements for a more comprehensive test of the hypothesis advanced by Burch et al. (2004). For most of the 12 cases tested, they found consistency between the rates of ionospheric and plasmaspheric drifts. However, for 2 cases the ionospheric drift rate was smaller than the plasmaspheric rate at the $>3\sigma$ level. No inconsistencies in the opposite sense ($\xi > 1$) were found. These two instances of significant differences between ionospheric and plasmaspheric drift rates suggest that, at least at some times, effects other than those described by Burch et al. (2004) may be important.

As a possible contributor to this apparent added complexity, Gallagher et al. (2005) propose a different mechanism that may lead to sub-corotation. They suggest that a dawn-dusk asymmetry in the electric potential, which results from gradients in Hall conductance at the terminators, can drive a net sub-corotational drift whose amplitude depends on storm phase. Both the ionospheric and plasmaspheric effects would be similar to those expected in the scenario described by Burch et al. (2004), so distinguishing between the two mechanisms in a way that permits establishing their relative importance proved to be elusive.

Burch et al. (2004) note that azimuthal drifts in the ionosphere have long been known, so corresponding motions in the plasmasphere should not be surprising. However, contemporary models of terrestrial magnetospheric convection do not take this effect into account. They further call attention to one specific result, namely that convection paths in the inner magnetosphere will be distorted. In particular, the boundary between open and closed convection paths will be closer to Earth than for a corotating plasmasphere. From a practical point of view, in situ and ground-based observations, which often must be interpreted using the implicit assumption of strict corotation, may wrongly attribute spatial variations to temporal variations. For example, pre-existing density structures carried into the "field of view" of ground-based measurements would look like a temporal variation to an observer not taking into account the possibility of plasma drifts from other longitudes.

It is finally interesting to note that large corotation lags are also observed in the magnetospheres of Jupiter and Saturn. These lags result from plasma mass loading in the vicinity of strong equatorial plasma sources present deep inside these magnetospheres and from the subsequent outward plasma transport via the centrifugal interchange instability that operates in these environments (Hill 1979). Despite their obvious differences, the same physical mechanism, the conservation of angular momentum (or equivalently the Coriolis force) of plasma elements transported outwards (mainly in the ionosphere of the Earth but also in relation with the plasmaspheric wind or in the equatorial plane of the giant planet magnetospheres), is important to the corotation lags in all three magnetospheres (Burch et al. 2004).

7 Shoulders, Channels, Fingers, Crenulations

Many other medium-scale density structures exist in the plasmasphere, but could not be clearly distinguished before data from the global imaging mission IMAGE and the four-spacecraft mission CLUSTER became available. New terms have therefore been given to those structures, like shoulders, channels, fingers and crenulations.

An example of previously unknown phenomena first detected by IMAGE is the shoulder (Burch et al. 2001a, 2001b). A shoulder appears as a sharp azimuthal gradient, which forms following sharp increases in activity. The shoulders are caused by the residual shielding of the convection electric field following the sudden weakening of convection when the IMF turns from southward to northward (Goldstein et al. 2002).

From a study on the evolution of a plume, Spasojević et al. (2003) demonstrated that the differential rotation of the western edge of a plume in L and the stagnation of the eastern edge, led to the wrapping of the plume around the main plasmasphere and to the formation of a low-density channel located between the plasmasphere and the plume. Figure 25 gives an example of such channel development on 10 June 2001 in the pre-midnight sector, when a plume wrapped around the main body of the plasmasphere (Sandel et al. 2003). A channel can extend over a few hours in MLT, with a width of $\sim$0.5 R_E.

Though the concept of plasmaspheric (or plume) phases is remarkably useful in providing a global context for data interpretation, this concept is far from a complete picture of plasmaspheric dynamics. On smaller scale, many stormtime features have yet to be explained; for example, crenulations are a few-tenths-R_E modulation of the plasmapause location that are often seen between the dawnside terminator and the westmost edge of a plume (Spasojević et al. 2003; Goldstein and Sandel 2005). Other complex structures appear during quiet conditions, but also remain without firm explanation. This unpredictability reflects an incomplete understanding of both inner magnetospheric electric fields and the quantitative influence of ULF waves and plasma instabilities on the distribution of cold plasma (Pierrard and Lemaire 2004).

Prior to 2000, several studies had noted the increased likelihood for medium-scale spatial structure during quieter intervals (Chappell 1974; Moldwin et al. 1994, 1995). This same tendency was also observed in data from IMAGE (Spasojević et al. 2003) and CLUSTER (Dandouras et al. 2005). Goldstein and Sandel (2005) suggested that the increase in structural complexity during early and deep recovery could be explained by consideration of flow streamlines: When flows are strong, streamlines are closer together, leading to a decreased scale size transverse to the flow. This would lead to a steeper plasmapause density gradient, and a more laminar plasmapause shape. On the other hand, the streamlines

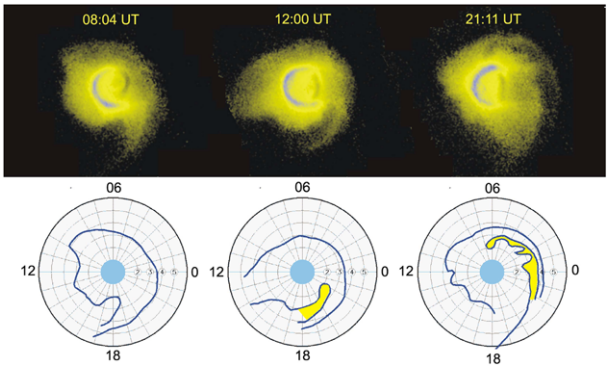

Fig. 25 (*Top*) EUV images on 10 June 2001 scaled to a common range and rotated so that the Sun is to the left. (*Bottom*) Mapping of the prominent brightness gradients onto the geomagnetic equator plane in [L,MLT] space; the *yellow fill* marks the channel. (Adapted from Sandel et al. 2003)

from weaker flows would be more widely spaced, and the transverse size of medium-scale structures would be larger, allowing for a more lumpy plasmapause. Even more puzzling are deep quiet features called fingers that have only tentatively been explained as arising from some resonance of ultra-low frequency waves (Adrian et al. 2004), but which also might be explained by interchange physics. Explaining medium-scale density features both inside and at the plasmapause is one of the major remaining challenges to closure in studies of plasmaspheric dynamics.

8 Small-Scale Density Irregularities

Field-aligned density irregularities have been observed since the discovery of the plasmasphere. But the IMAGE mission, and in particular the RPI instrument, made it possible to more precisely characterize those density structures. Note that the EUV instrument onboard IMAGE does not observe density structures less than its spatial resolution of about 0.1 R_E. Thanks to the high resolution, in space and time, of the WHISPER instrument, the CLUSTER mission gives also new results on the morphology, dynamics and occurrence of small-scale density irregularities.

8.1 Earlier Work

8.1.1 Field-Aligned Density Irregularities

The existence of field-aligned density irregularities capable of guiding whistler-mode waves for long distances in the magnetosphere has been known since the early 1960s (e.g., Smith 1961; Helliwell 1965), becoming well established through ground-based whistler observations at a wide range of latitudes. Propagation of whistlers between conjugate hemispheres along multiple discrete paths was found to occur regularly at some longitudes even under prolonged quiet conditions, but tended to be poorly defined or undetectable during the highest levels of disturbance. The apparent lifetimes of individual paths could be as long as several hours and the instantaneous distributions of paths in latitude or L value, as determined from ground whistler stations, tended to be unchanged on a time scale of a few minutes (see Hayakawa 1995). Meanwhile, also in the 1960s, topside sounders showed clear evidence of field-aligned propagation of free-space-mode waves back and forth between the sounder and reflection points in the conjugate hemisphere (e.g., Muldrew 1963; Loftus et al. 1966).

The irregularities involved in both ground-based and satellite studies were not usually detected directly, but instead were studied indirectly through their transmission properties as wave ducts or guides. Theory as well as limited experimental evidence indicated that the irregularities involved step-like changes or local enhancements in the range 1–30% with respect to the average density background (e.g., Smith 1961; Booker 1962; Strangeways and Rycroft 1980; Platt and Dyson 1989). For whistler propagation, density enhancement ducts, capable of internally trapping and guiding waves, were inferred to be of order 10 to 20 km in cross section near the ionosphere (e.g., Helliwell 1965). On a rare OGO 3 satellite pass, Angerami (1970) found evidence of whistlers that were trapped within ducts as well as of whistler wave energy escaping from ducts at frequencies above the local electron gyrofrequency. The observations suggested that the equatorial duct cross sections near $L = 4$ were several hundred kilometers.

The origin of the magnetospheric irregularities guiding whistler and sounder waves within the plasmasphere has not been well established. Proposed mechanisms for whistler ducts include irregular electric fields that give rise to flux tube interchange (Cole 1971; Thomson 1978) and thundercloud electric fields (Park and Helliwell 1971).

8.1.2 Irregular Density Structures in the Outer Plasmasphere

Satellite in situ density measurements, for example by LANL (e.g., Moldwin et al. 1995) and CRRES (e.g., Fung et al. 2000), revealed concentrations of irregularities in the plasmapause region, some of which appear to trap and guide whistler-mode waves (Koons 1989). These structures appear to vary widely in cross section, ranging from 50 km upward. Due to limitations on spatial sampling rates, the bulk of the reports made thus far concern features with cross sections of order hundreds of kilometers. Observed peak to valley density ratios for these features vary from ∼1.2 to 5 or more.

The presence in the middle to outer plasmasphere of density variations with scale widths of thousands of kilometers has been known from whistler studies since the 1970s (e.g., Park and Carpenter 1970; Park 1970). On occasion, such irregularities are seen in a belt in the outer plasmasphere that terminates abruptly about 1 R_E inward from the plasmapause (Carpenter and Lemaire 1997). Within such a belt the peak densities tend to reach the quiet plasmasphere level while the minima may be lower than the peaks by factors of as much as 5. Longitudinal variations in density by factors of up to 3 in longitude have been found to arise in the aftermath of magnetic disturbances (Park and Carpenter 1970). Little is known of the occurrence rates and distributions on a global scale of these types of irregularities in the outer plasmasphere.

A number of instabilities have been suggested to explain the irregular density structures observed in the plasmasphere: the drift wave instability (e.g., Hasegawa 1971), the Rayleigh Taylor instability (e.g., Kelley 1989), the pressure gradient instability (e.g., Richmond 1973), and the gravitational interchange instability (e.g., Lemaire 1975).

8.2 Remote Sensing of Density Irregularities by the RPI Instrument

8.2.1 Comments on RPI Observations

The IMAGE mission provided the first opportunity to study the response of the plasmasphere to high power radio sounding by RPI. In planning for the IMAGE mission, it was expected that irregular density structure would be encountered, particularly in the plasmapause region. However, it was not anticipated that the plasmasphere boundary layer (PBL) would consistently appear as a rough surface to the sounder. It was not anticipated that sounder echoes received near or within the plasmasphere would fall into two quite different categories: Discrete echoes that had followed magnetic field-aligned paths and diffuse or "direct" echoes that had propagated generally earthward, in directions not initially aligned with the magnetic field (Carpenter et al. 2002).

Figure 26 illustrates these points by a series of six "plasmagrams", obtained 4 minutes apart as IMAGE approached and then penetrated the plasmasphere along the orbit shown schematically on the right of the figure. The plasmapause was estimated to be at $L = 4.1$. The records display echo intensity on a gray scale in coordinates of virtual range (0.3 to 4.2 R_E, assuming propagation at velocity c along ray paths to reflection points) versus sounder frequency (40 to 600 kHz). Two different types of echoes are observed on those plasmagrams: the "field-aligned echo" and the "plasmasphere echo". Field-aligned echoes

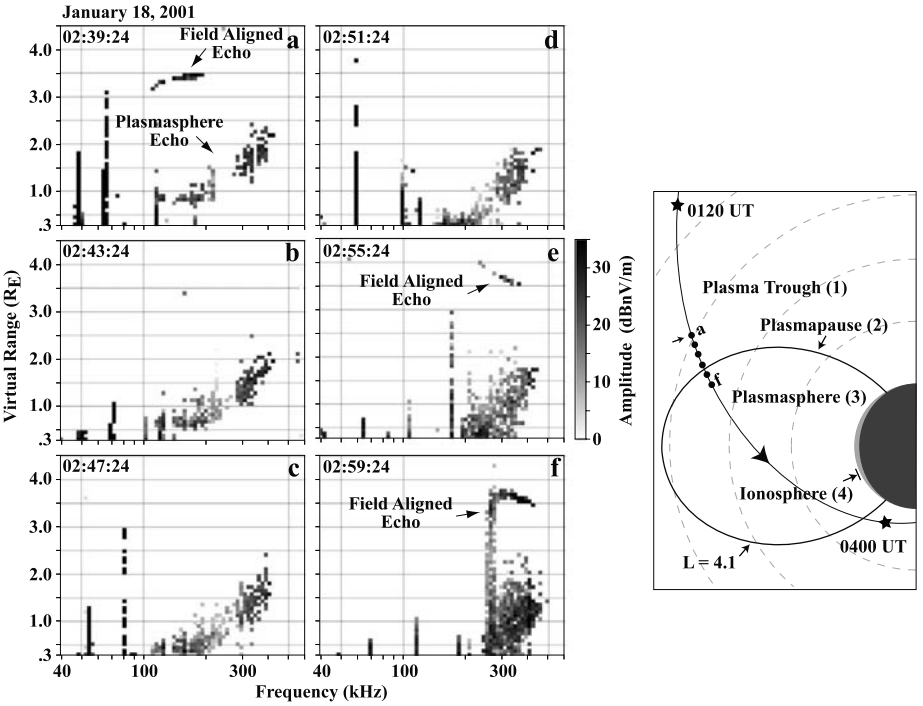

Fig. 26 A series of six soundings by RPI showing range spreading of echoes interpreted as evidence of irregular density structure in both the PBL and outer plasmasphere. The soundings were performed as IMAGE approached and penetrated the plasmasphere along the orbit shown schematically on the *right*. (Adapted from Carpenter et al. 2002)

were seen both outside the plasmasphere (panel a) and just inside the plasmapause (panels e and f), while a direct echo appears during each sounding. The striking differences in range-versus-frequency form between the former and the latter reflect the differences in the electron density profiles along the respective propagation paths. The field-aligned echo pulses encountered smooth density profiles and small initial gradients while propagating along relatively long paths of order 4 R_E in length. Meanwhile, the direct-echo pulses encountered gradients from the PBL inward that were steeper by comparison. Those pulses returned from closer turn-around points, and from the PBL inward encountered widespread field-aligned irregularities. The irregularities gave rise to scattering along the entire path from the near vicinity of IMAGE (so-called "zero range" scattering) to the most distant turning point. Hence the returning echoes tended to be widely spread in range at each frequency.

Within the plasmasphere at $L \geq 2.5$, diffuse echoes were observed on essentially every sounding. The upper frequency limit for zero range echo components increased from a typical value of ~200 kHz in the outer plasmasphere to ~800 kHz near $L = 2.5$ in the inner plasmasphere. Discrete, field-aligned echoes were observed, but not on every sounding. Within the plasmasphere at $L < 2.5$ the non field-aligned or direct echoes tended to exhibit less range spreading than at $L > 2.5$.

8.2.2 Interpretation of RPI Observations in Terms of Density Structure

The plasma trough along high-latitude field lines appears to contain sufficient field-aligned structure to guide discrete X-mode waves over distances of 4 or 5 R_E down to lower alti-

tudes. When this filamentary structure is present, it is found over extensive regions exterior to the PBL. The plasma trough under most conditions appears to be a smooth medium at wavelengths in the vicinity of 200–800 m, which corresponds to the half wavelength of the waves that propagate across the magnetic field in the region without giving rise to detectable echoes.

The PBL regularly contains embedded irregularities that are distributed both in equatorial radius and, more importantly, in longitude, thus giving rise to aspect sensitive scattering of RPI pulses and very possibly to tunneling. The echoes can extend in range beyond a well defined minimum by as much as 1 R_E when coherent signal integration is used. RPI confirmed earlier suggestions that density irregularities tend to be concentrated in the PBL and showed that such concentrations nearly always exist.

Strong scattering in the plasmasphere, particularly of the zero range type, presumably occurs in the presence of irregularities that are about half the probing wavelength in size. Hence it is found that the outer plasmasphere, beyond $L \approx 2.5$, is regularly permeated by field-aligned irregularities with scale widths in the range 200–800 m. The plasmasphere beyond $L \approx 2.5$ also exhibits a class of field-aligned irregularities that have been identified from evidence of propagation within irregularities rather than at large angles to the magnetic field. The inferred scale widths vary from 1 to 10 km, based on the assumption that structures several wave lengths across are needed to trap and guide the field-aligned X-mode echoes that are frequently observed from RPI. Earlier studies (noted above) of the conditions for trapping of such waves (or whistler-mode waves) by or within such field-aligned density irregularities found that the density levels within the irregularities remained within a range 1–30% of the nearby background.

8.3 In situ Observations of Small-Scale Density Structures

CLUSTER observations confirmed that small-scale density structures, or density irregularities, are often present in the outer plasmasphere, near the Roche Limit surface associated with hydrodynamic instability (Décréau et al. 2005). It is, however, quite difficult to assess the shape of a density irregularity or its relative motion with respect to the background, even with a four-spacecraft constellation.

8.3.1 Morphology

Are density irregularities field-aligned? What is their size along and across magnetic field lines? CLUSTER observations can address those questions directly. Décréau et al. (2005) considered one event (13 June 2001, meridian cut around 17:00 MLT) with three spacecraft near the same modelled magnetic field line (CLUSTER constellation as in Fig. 2b). The same complex specific signature is recognized in density profiles (shown versus R_{equat} in Fig. 27) measured from the three conjugate spacecraft, C2, C1 and C4 within a 2.5 minutes time interval. A remnant form of the signature is encountered 40 minutes later by the fourth satellite, C3: The main density dip (black circle) can be correlated with a similar feature seen in each of the C2, C1 and C4 signatures.

Those observations can be interpreted in the framework of a rigid plasmasphere. The common structure (the main dip) would in that case extend up to the longitude of C3 (C2, C4, C1 and C3 are placed at increasing respective longitudes, within 1° total). Features correlated only on C2, C1, C4, like the two small bumps seen just above the main dip (i.e., at higher R_{equat}), would be restricted to the longitude range of the trio. Subtle differences observed between the conjugate spacecraft (like a small dip at $R_{\text{equat}} = 4.9\ R_E$ seen only

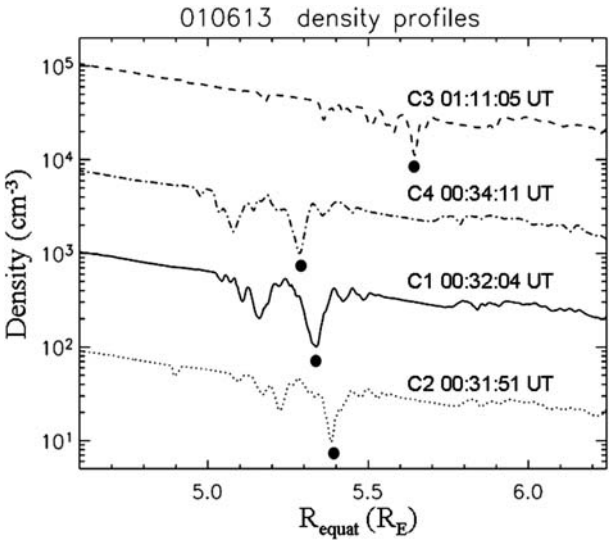

Fig. 27 Density profiles from WHISPER are shown as a function of R_{equat} for a structure crossed around 00:35 UT during the plasmasphere pass on 13 June 2001 (same event as in Fig. 11). The density values have been multiplied by factors, respectively 8, 64 and 512 for C1, C4 and C3. (Adapted from Décréau et al. 2005)

on C2) could be attributed to small filamentary structures which are not encountered by all spacecraft.

Alternatively, the different morphology of the structure observed by C3, as compared to the one observed by C2, C4 and C1, could be attributed to a time effect. In particular, interchange velocity values at work in hydrodynamic instability are proportional to the depth (or amplitude) of a density irregularity (see Lemaire and Gringauz 1998, p. 263) The main dip would then travel faster and reach higher geocentric distances than small bumps part of the structure, leading thus to the observed shape.

8.3.2 Dynamics

The time delay method provides the orientation of a given density structure, as well as its velocity along its normal, assuming this structure to be locally planar (De Keyser et al. 2008, this issue). It is possible to apply this method in the outer plasmasphere when the spacecraft are configured at 100 km separation. In practice, the configuration is elongated along the orbit, the largest distances respectively along and transverse to the orbit are ∼300 km and ∼60 km. Three event studies used the time delay method to explore motions of density structures in the outer plasmasphere.

The first event (Décréau et al. 2005) is located in the dusk region, where corotation and convection are competing (inducing velocities in opposite directions). The authors present a detailed shape of a density structure observed at $L \approx 6$ during this event. The estimated velocity components (-2, 0.7, 0.5 km s^{-1} in geocentric solar ecliptic, GSE, coordinates) indicate that corotation dominates, in this case. Magnetic activity is actually low during the day preceding and including the event ($Dst \approx -10$ nT), which explains why the plasmasphere is expanded and its outer edge corotating.

The second event (Darrouzet et al. 2004) is located in the pre-midnight sector. A plasmaspheric plume is seen in the inbound and outbound passes, and many small-scale density structures are visible inside the plasmasphere. By combining density gradient analysis and time delay method, the authors found that the major component of the boundary velocity of a density irregularity corresponds to corotation.

In the third event (Décréau 2008, personal communication), multiple density structures are encountered in the post-midnight sector on 8 February 2002 near perigee. Most irregularities are present on the four density profiles. Focusing on a double structure at the start of the time interval, the time delay method gives the velocity components associated to the first outer density peak. Those values are consistent with velocity components derived by the EDI instrument, indicating that in this case the plasma and its boundary move at comparable velocities.

8.3.3 Occurrence

In an analysis of 264 plasmasphere passes, Darrouzet et al. (2004) identified density irregularities by a density depletion ratio of at least 10%. This survey suggests that there are more density irregularities in the dawn, afternoon and post-dusk MLT sectors. Two of these sectors correspond to the sectors where the plasmapause tends to be thicker. The transverse equatorial size and density depletion ratio distributions of density irregularities are exponential with a characteristic size of 365 km and a characteristic density ratio of 20%. The larger ones (in size) are observed when K_p is small. This is in part due to the fact that large ones simply cannot exist when the plasmasphere is small for high K_p. As expected, there are more density irregularities during and after periods of high geomagnetic activity, suggesting that they are generated near dusk by variations in the convection electric field. But this sample has few cases with high K_p and is therefore biased in this respect.

9 Conclusion

The CLUSTER and IMAGE missions provide a new and non-local view of the plasmasphere, thanks to the new capabilities of those missions: global imaging with IMAGE and four-spacecraft in situ measurements with CLUSTER. Using advanced imaging techniques and radio sounding, IMAGE provided new results for the global density structure and behaviour of plasma in the plasmasphere, while multipoint tools applied to CLUSTER data gave new opportunities to analyse the geometry and motion of plasmaspheric density structures. Refilling has been studied in detail, new results on ion composition have been derived, and new views of plasmaspheric structures have been obtained and analysed in new ways.

9.1 Sources and Losses in the Plasmasphere

Sandel and Denton (2007) updated our view of refilling by analysing IMAGE data during a 70 hours quiet period. They found an orderly increase in He^+ column abundance with time, which slowed near the end of the period. Gallagher et al. (2005) quantitatively obtained the He^+ refilling rates at the equator. Tu et al. (2005) demonstrated that the parallel electron velocity is almost constant along field lines in the inner plasmasphere. Darrouzet et al. (2006b) found that there is no evidence for sharp density gradients along field lines, such as would be expected in refilling shock fronts propagating along field lines. This extensive body of evidence suggests that refilling of flux tubes is a gradual process as described by Lemaire (1989) and Wilson et al. (1992).

The plasmasphere rarely appears filled to saturation, i.e., in diffusive equilibrium with the ionosphere. Reinisch et al. (2004) found significant refilling in less than 28 hours near $R = 2.5\ R_E$, but still insufficient to reach saturation levels. Cases of smooth density transition from the plasmasphere to the subauroral region without a distinct plasmapause have been

observed in 10% of the RPI database (Tu et al. 2007). This long refilling time and this smooth transition could be explained if the plasmasphere experiences a slow outward drift in addition to corotation and convection: the plasmaspheric wind (Lemaire and Schunk 1992). Dandouras (2008) showed with CIS data that systematically more ions are going outwards than inwards in the plasmasphere, at all LT. This could be the first direct evidence of the plasmaspheric wind.

New insights into the plasmaspheric erosion process have been given by IMAGE observations. The typical erosion cycle, including the formation of plumes, are followed through EUV images (Goldstein and Sandel 2005). Dramatic evidence confirming the effects of erosion were provided by RPI observations showing that outer plasmaspheric flux tubes could lose more than two thirds of their plasma in less than 14 hours (Reinisch et al. 2004).

9.2 Overall Plasma Distribution and Ion Composition

The global images by EUV improved our understanding of the distribution of plasma in the plasmasphere and the forces that control it. The sounding measurements from RPI provided field-aligned electron density profiles, which allow to build 2-D electron density images along the satellite orbit (Tu et al. 2005). Such images are useful to differentiate various plasma regions in the near-Earth magnetosphere and to provide insight into the plasma dynamics in those regions.

CLUSTER contributed the first systematic determination of spatial gradients of plasmaspheric density (Darrouzet et al. 2006b; De Keyser et al. 2007). This has produced an overall view of the geometry of the electron density distribution in the outer plasmasphere. It allows an evaluation of the relative importance of the dominant density gradients inside the plasmasphere: the increase of density along field lines away from the equator and its decrease away from Earth. The overall density structure is mainly aligned and slowly varying with the magnetic field at low *MLAT*, $\pm 30°$ (see also the IMAGE study by Reinisch et al. 2001), with pronounced transverse density variation.

By combining observations from the ground and He^+ column abundances from EUV, the ratio He^+/H^+ in the plasmasphere has been derived. Clilverd et al. (2003) inferred a ratio of $\sim$3.8% for an event with moderate geomagnetic disturbance, while Grew et al. (2007) found a value of $\sim$18% in the case of a prolonged geomagnetic disturbance. The presence of O^+ has also been confirmed. Using CIS data, Dandouras et al. (2005) observed mostly similar density profiles for H^+ and He^+ ions, with the He^+ densities being lower by a factor of $\sim$15. O^+ are not observed as part of the main plasmaspheric population at the CLUSTER altitudes at a significant level. Low-energy ($<$25 eV) O^+ are observed as upwelling ions, escaping from the ionosphere along auroral field lines. O^{++} can also be observed in these upwelling ion populations. Low-energy O^+ have been observed in some plasmaspheric plumes, exhibiting symmetric bi-directional pitch-angle distributions and having an outward expansion velocity.

9.3 Plasmaspheric Plumes

EUV images demonstrate that plumes form and develop in three phases (sunward surge, plume narrowing, plume rotating) that are directly correlated with relative increases or decreases in geomagnetic activity (Goldstein and Sandel 2005). This has been confirmed in many studies using EUV data, with and without in situ measurements (Goldstein et al. 2004b; Spasojević et al. 2004; Kim et al. 2007). However, during post-storm recovery and on smaller scales, our predictive capability remains limited.

Plasmaspheric plumes have also been routinely observed by the CLUSTER spacecraft. In the case of large satellites separation, a comparative study between each crossing clearly illustrates the global shape of a plume (Darrouzet et al. 2008). In some situation, CLUSTER observes details of the formation of a large-scale plume, where filamentary density structures are dragged from the near-Earth foot of the plume. Direct, complementary comparison with EUV images can then be done: It gives a consistent picture for radial position and MLT extent of plumes (Darrouzet et al. 2006a).

In the case of small separation between the CLUSTER satellites, multipoint tools can be used to study the geometry and motion of plumes. Darrouzet et al. (2006a) found the foot of the plume attached to the plasmasphere and nearly corotating, but with the extended plume moving outward and lagging further behind corotation. From a comparative study between the inbound and outbound plume crossing Darrouzet et al. (2008) found the plume rotated eastward and moved to higher L values. Between both passes CLUSTER was displaced outward along the plume, which narrowed and lowered in density. The mean apparent radial velocity was found to be $\sim$0.25 km s^{-1}.

From a statistical point of view, plasmaspheric plumes are found to be a common feature observed in the outer plasmasphere, mainly in the afternoon and pre-midnight MLT sectors (Darrouzet et al. 2008). A small increase of geomagnetic activity is sufficient to produce plumes. Denser plumes are observed especially at small L (around 5–7 R_E) and in all MLT sectors (except morning), mostly pre-midnight.

Plasmaspheric plume signatures have also been detected in the ionosphere, in particular with TEC measurements (Foster et al. 2002). TEC signatures of plumes are more common in the North American sector, though weaker plume signatures are seen over Europe and Asia (Yizengaw et al. 2008). It has been demonstrated that plumes play a crucial role in mid-latitude ionospheric density enhancements (Yizengaw et al. 2006), polar ionization patches (Su et al. 2001) and are strongly correlated with the loss of ring current ions (Burch et al. 2001b).

9.4 Density Structures at Smaller Scales

Notches are one of the remarkable large-scale structural features of the plasmasphere, only recognized after flight of the EUV instrument. Notches can extend over more than 2 R_E in radial distance and 3 hours MLT in the magnetic equatorial plane (Gallagher et al. 2005). They have been observed to persist for periods as long as 60 hours (Sandel et al. 2003). Notches are also observed by WHISPER, very often associated with both continuum radiation and intense electrostatic emissions (Décréau et al. 2004).

Sandel et al. (2003) found that the outer plasmasphere, as traced by notches, rotates at a rate significantly slower ($\sim$10%) than corotation. Burch et al. (2004) suggest that this corotation lag is caused by the ionospheric disturbance dynamo. Gallagher et al. (2005) find that additional mechanisms may be needed such as Hall conductance gradients at the terminators that cause a dawn-dusk electric potential asymmetry, which also yields a net sub-corotational plasmaspheric drift.

The IMAGE and CLUSTER missions revealed many other medium-scale density structures in the plasmasphere that could not be clearly distinguished before: shoulders, channels, fingers and crenulations. For example, a shoulder can be formed after a sharp decrease of geomagnetic activity (Pierrard and Cabrera 2005); fingers appear to result from quite-time global magnetospheric oscillations (Adrian et al. 2004); crenulations are seen as a modulation of the plasmapause location (Spasojević et al. 2003).

IMAGE provided the first opportunity to study the response of the plasmasphere to high power radio sounding by the RPI instrument (Carpenter et al. 2002). Two different types

of sounder echoes have been observed: Discrete echoes that have followed geomagnetic field-aligned paths and diffuse echoes that have returned to the satellite along ray paths that extended generally earthward from the satellite. The reflection points of the diffuse echoes are in the PBL or in the plasmasphere interior, while the discrete echoes follow field-aligned density irregularities that are common in low and high-latitude magnetospheric regions. Field-aligned irregularities in electron density are within $<10\%$ of background, with cross-field scale sizes between 200 m and >10 km.

The CLUSTER constellation has also identified field-aligned density structures in the outer plasmasphere. The spatial extent along the magnetic field is larger than the spacecraft separation in that direction. Sizes transverse to the field in a meridian plane are found to range from $\sim$10 km to a few 100 km. Those length scales vary with the altitude of observation. Sizes in the third dimension (in longitude) can be very small, down to 20 km (Décréau et al. 2004). Undulations in longitude, a known feature of the plasmapause, are not easily distinguished with the CLUSTER spacecraft, which travel along polar orbits. The primary motion of small-scale density structures is found to be corotation (Darrouzet et al. 2004). From a statistical study, Darrouzet et al. (2004) established that density irregularities are often, though not always, seen in the plasmasphere and at the plasmapause. They have a transverse equatorial size that falls off exponentially with a characteristic value of 365 km and going up to 5000 km. There are more density irregularities when the level of geomagnetic activity is higher. There seems to be an MLT asymmetry in their distribution.

9.5 Perspectives

Much progress in our understanding of plasmaspheric density structures has been made with the CLUSTER and IMAGE missions, but many questions remain unsolved. For example, the coupling between the ionosphere and the plasmasphere through refilling and erosion is not yet completely understood; several mechanisms for the formation of plumes have been proposed, but their relative importance is not yet clear; many medium-scale density structures (like fingers or channels) are not fully explained; the distributions of field-aligned density structures in space and time throughout the plasmasphere are not yet well documented; the mechanisms that create small-scale density irregularities are not yet fully understood.

The CLUSTER mission has been extended until December 2009. Interestingly for plasmaspheric studies, the orbit is changing since June 2007 towards a lower perigee (down to 2.5 R_E). This will allow the study of the inner plasmasphere. With the new orbit, it should also be possible to observe plasmaspheric plumes extending up to the magnetopause. But, sadly, the IMAGE satellite was lost on 18 December 2005. There is now a lack of global imaging of the plasmasphere, which could be filled in the coming years with China's CHANG'E and KUAFU missions. More recent multi-spacecraft missions visit the plasmasphere, such as THEMIS, though this region is not their primary goal and their instrumentation is not specifically adapted for studying it. The Canadian ORBITALS (Outer Radiation Belt Injection, Transport, Acceleration and Loss Satellite) mission is a dedicated inner magnetosphere mission, under preparation, and will carry plasma instrumentation for in situ plasmasphere measurements. The ERG (Energization and Radiation in Geospace) project has been proposed to the Japan Space Agency. But, no other dedicated inner magnetosphere mission is on the horizon, although one, WARP, has been proposed in the frame of ESA's Cosmic Vision program.

Acknowledgements The IMF Y and Z components and the K_p and *Dst* indices were provided by the Space Environment Information System, SPENVIS (http://www.spenvis.oma.be). The *am* index was provided by the International Service of Geomagnetic Indices, ISGI (http://isgi.cetp.ipsl.fr). F. Darrouzet and J.

De Keyser acknowledge the support by the Belgian Federal Science Policy Office (BELSPO) through the ESA/PRODEX project (contract 13127/98/NL/VJ (IC)). F. Darrouzet thanks M. Roth for careful reading of the manuscript. Work at Dartmouth College was supported by U.S. National Science Foundation grants ATM-0632740 and ATM-0120950 (Center for Integrated Space Weather Modeling funded by the Science and Technology Centers Program). Work at The University of Arizona was funded by a subcontract from Southwest Research Institute under NASA contract NAS5-96020 with SwRI, and by NASA Grant NNX07AG46G. This paper is an outcome of the workshop "The Earth's plasmasphere: A CLUSTER, IMAGE, and modeling perspective", organized by the Belgian Institute for Space Aeronomy in Brussels in September 2007.

References

S. Abe, H. Kawano, J. Goldstein, S. Ohtani, S.I. Solovyev, D.G. Baishev, K. Yumoto, Simultaneous identification of a plasmaspheric plume by a ground magnetometer pair and IMAGE Extreme Ultraviolet Imager. J. Geophys. Res. **111**, A11202 (2006)

M.L. Adrian, D.L. Gallagher, L.A. Avanov, IMAGE EUV observation of radially bifurcated plasmaspheric features: First observations of a possible standing ULF waveform in the inner magnetosphere. J. Geophys. Res. **109**, A01203 (2004)

N. André, J.F. Lemaire, Convective instabilities in the plasmasphere. J. Atmos. Sol.-Terr. Phys. **68**(2), 213–227 (2006)

J.J. Angerami, Whistler duct properties deduced from VLF observations made with the Ogo 3 satellite near the magnetic equator. J. Geophys. Res. **75**(31), 6115–6135 (1970)

M. Blanc, A.D. Richmond, The ionospheric disturbance dynamo. J. Geophys. Res. **85**(A4), 1669–1686 (1980)

H.G. Booker, Guidance of radio and hydromagnetic waves in the magnetosphere. J. Geophys. Res. **67**(11), 4135–4162 (1962)

J.E. Borovsky, M.H. Denton, A statistical look at plasmaspheric drainage plumes. J. Geophys. Res. **113**, A09221 (2008)

J.E. Borovsky, M.F. Thomsen, D.J. McComas, T.E. Cayton, D.J. Knipp, Magnetospheric dynamics and mass flow during the November 1993 storm. J. Geophys. Res. **103**(A11), 26373–26394 (1998)

P.C. Brandt, D.G. Mitchell, Y. Ebihara, B.R. Sandel, E.C. Roelof, J.L. Burch, R. Demajistre, Global IMAGE/HENA observations of the ring current: Examples of rapid response to IMF and ring current-plasmasphere interaction. J. Geophys. Res. **107**(A11), 1359 (2002)

K. Bullough, J.L. Sagredo, Longitudinal structure in the plasmapause: VLF goniometer observations of knee-whistlers. Nature **225**(5237), 1038–1039 (1970)

J.L. Burch, IMAGE mission overview. Space Sci. Rev. **91**(1–2), 1–14 (2000)

J.L. Burch, S.B. Mende, D.G. Mitchell, T.E. Moore, C.J. Pollock, B.W. Reinisch, B.R. Sandel, S.A. Fuselier, D.L. Gallagher, J.L. Green, J.D. Perez, P.H. Reiff, Views of Earth's magnetosphere with the IMAGE satellite. Science **291**, 619–624 (2001a)

J.L. Burch, D.G. Mitchell, B.R. Sandel, P.C. Brandt, M. Wüest, Global dynamics of the plasmasphere and ring current during magnetic storms. Geophys. Res. Lett. **28**(6), 1159–1162 (2001b)

J.L. Burch, J. Goldstein, B.R. Sandel, Cause of plasmasphere corotation lag. Geophys. Res. Lett. **31**, L05802 (2004)

P. Canu, P.M.E. Décréau, J.G. Trotignon, J.L. Rauch, H.C. Séran, P. Fergeau, M. Lévêque, P. Martin, F.X. Sené, E. Le Guirriec, H. Alleyne, K. Yearby, Identification of natural plasma emissions observed close to the plasmapause by the Cluster-Whisper relaxation sounder. Ann. Geophys. **19**(10–12), 1697–1709 (2001)

D.L. Carpenter, New experimental evidence of the effect of magnetic storms on the magnetosphere. J. Geophys. Res. **67**(1), 135–145 (1962)

D.L. Carpenter, Whistler evidence of a "knee" in the magnetospheric ionization density profile. J. Geophys. Res. **68**(6), 1675–1682 (1963)

D.L. Carpenter, Whistler Evidence of the Dynamic Behavior of the Duskside Bulge in the Plasmasphere. J. Geophys. Res. **75**(19), 3837–3847 (1970)

D.L. Carpenter, Some aspects of plasmapause probing by whistlers. Radio Sci. **18**(6), 917–925 (1983)

D.L. Carpenter, R.R. Anderson, An ISEE/Whistler model of equatorial electron density in the magnetosphere. J. Geophys. Res. **97**(A2), 1097–1108 (1992)

D.L. Carpenter, J. Lemaire, Erosion and recovery of the plasmasphere in the plasmapause region. Space Sci. Rev. **80**(1–2), 153–179 (1997)

D.L. Carpenter, J. Lemaire, The plasmasphere boundary layer. Ann. Geophys. **22**(12), 4291–4298 (2004)

D.L. Carpenter, B.L. Giles, C.R. Chappell, P.M.E. Décréau, R.R. Anderson, A.M. Persoon, A.J. Smith, Y. Corcuff, P. Canu, Plasmasphere dynamics in the duskside bulge region: A new look at an old topic. J. Geophys. Res. **98**(A11), 19243–19271 (1993)

D.L. Carpenter, R.R. Anderson, W. Calvert, M.B. Moldwin, CRRES observations of density cavities inside the plasmasphere. J. Geophys. Res. **105**(A10), 23323–23338 (2000)

D.L. Carpenter, M.A. Spasojević, T.F. Bell, U.S. Inan, B.W. Reinisch, I.A. Galkin, R.F. Benson, J.L. Green, S.F. Fung, S.A. Boardsen, Small-scale field-aligned plasmaspheric density structures inferred from the Radio Plasma Imager on IMAGE. J. Geophys. Res. **107**(A9), 1258 (2002)

C.R. Chappell, Recent satellite measurements of the morphology and dynamics of the plasmasphere. Rev. Geophys. Space Phys. **10**(4), 951–979 (1972)

C.R. Chappell, Detached Plasma Regions in the Magnetosphere. J. Geophys. Res. **79**(13), 1861–1870 (1974)

C.R. Chappell, K.K. Harris, G.W. Sharp, The morphology of the bulge region of the plasmasphere. J. Geophys. Res. **75**(19), 3848–3861 (1970a)

C.R. Chappell, K.K. Harris, G.W. Sharp, A study of the influence of magnetic activity on the location of the plasmapause as measured by OGO 5. J. Geophys. Res. **75**(1), 50–56 (1970b)

A.J. Chen, J.M. Grebowsky, Plasma Tail Interpretations of Pronounced Detached Plasma Regions Measured by Ogo 5. J. Geophys. Res. **79**(25), 3851–3855 (1974)

S.H. Chen, T.E. Moore, Magnetospheric convection and thermal ions in the dayside outer magnetosphere. J. Geophys. Res. **111**, A03215 (2006)

A.J. Chen, R.A. Wolf, Effects on the plasmasphere of a time-varying convection electric field. Planet. Space Sci. **20**(4), 483–509 (1972)

M.A. Clilverd, A.J. Smith, N.R. Thomson, The annual variation in quiet time plasmaspheric electron density, determined from whistler mode group delays. Planet. Space Sci. **39**(7), 1059–1067 (1991)

M.A. Clilverd, F.W. Menk, G. Milinevski, B.R. Sandel, J. Goldstein, B.W. Reinisch, C.R. Wilford, M.C. Rose, N.R. Thomson, K.H. Yearby, G.J. Bailey, I.R. Mann, D.L. Carpenter, In-situ and ground-based intercalibration measurements of plasma density at L = 2.5. J. Geophys. Res. **108**(A10), 1365 (2003)

M.A. Clilverd, N.P. Meredith, R.B. Horne, S.A. Glauert, R.R. Anderson, N.R. Thomson, F.W. Menk, B.R. Sandel, Longitudinal and seasonal variations in plasmaspheric electron density: Implications for electron precipitation. J. Geophys. Res. **112**, A11210 (2007)

K.D. Cole, Formation of field-aligned irregularities in the magnetosphere. J. Atmos. Terr. Phys. **33**, 741–750 (1971)

P.D. Craven, D.L. Gallagher, R.H. Comfort, Relative concentration of He^+ in the inner magnetosphere as observed by the DE 1 retarding ions mass spectrometer. J. Geophys. Res. **102**(A2), 2279–2289 (1997)

I. Dandouras, Detection of plasmaspheric wind by analysis of ion measurements obtained onboard the Cluster spacecraft. Geophys. Res. Abstr. **10**, 5360 (2008)

I. Dandouras, V. Pierrard, J. Goldstein, C. Vallat, G.K. Parks, H. Rème, C. Gouillart, F. Sevestre, M. McCarthy, L.M. Kistler, B. Klecker, A. Korth, M.B. Bavassano-Cattaneo, P. Escoubet, A. Masson, Multipoint observations of ionic structures in the plasmasphere by CLUSTER-CIS and comparisons with IMAGE-EUV observations and with model simulations, in *Inner Magnetosphere Interactions: New Perspectives from Imaging*, ed. by J. Burch, M. Schulz, H. Spence. Geophysical Monograph Series, vol. 159 (American Geophysical Union, Washington, 2005), pp. 23–53

F. Darrouzet, Etude de la magnétosphère terrestre par l'analyse multipoint des données de la mission CLUSTER. Contributions à la caractérisation des frontières et de la magnétosphère interne. PhD thesis, University of Orléans, France, 2006

F. Darrouzet, P.M.E. Décréau, J. De Keyser, A. Masson, D.L. Gallagher, O. Santolík, B.R. Sandel, J.G. Trotignon, J.L. Rauch, E. Le Guirriec, P. Canu, F. Sedgemore, M. André, J.F. Lemaire, Density structures inside the plasmasphere: Cluster observations. Ann. Geophys. **22**(7), 2577–2585 (2004)

F. Darrouzet, J. De Keyser, P.M.E. Décréau, D.L. Gallagher, V. Pierrard, J.F. Lemaire, B.R. Sandel, I. Dandouras, H. Matsui, M. Dunlop, J. Cabrera, A. Masson, P. Canu, J.G. Trotignon, J.L. Rauch, M. André, Analysis of plasmaspheric plumes: CLUSTER and IMAGE observations. Ann. Geophys. **24**(6), 1737–1758 (2006a)

F. Darrouzet, J. De Keyser, P.M.E. Décréau, J.F. Lemaire, M.W. Dunlop, Spatial gradients in the plasmasphere from Cluster. Geophys. Res. Lett. **33**, L08105 (2006b)

F. Darrouzet, J. De Keyser, P.M.E. Décréau, F. El Lemdani-Mazouz, X. Vallières, Statistical analysis of plasmaspheric plumes with CLUSTER/WHISPER observations. Ann. Geophys. **26**(8), 2403–2417 (2008)

J. De Keyser, F. Darrouzet, M.W. Dunlop, P.M.E. Décréau, Least-squares gradient calculation from multipoint observations of scalar and vector fields: Methodology and applications with cluster in the plasmasphere. Ann. Geophys. **25**(4), 971–987 (2007)

J. De Keyser, D.L. Carpenter, F. Darrouzet, D.L. Gallagher, J. Tu, CLUSTER and IMAGE: New ways to study the Earth's plasmasphere. Space Sci. Rev. (2008, this issue)

P.M.E. Décréau, D. Carpenter, C.R. Chappell, R.H. Comfort, J. Green, R.C. Olsen, J.H. Waite Jr., Latitudinal plasma distribution in the dusk plasmaspheric bulge: Refilling phase and quasi-equilibrium state. J. Geophys. Res. **91**(A6), 6929–6943 (1986)

P.M.E. Décréau, P. Fergeau, V. Krasnosels'kikh, M. Lévêque, Ph. Martin, O. Randriamboarison, F.X. Sené, J.G. Trotignon, P. Canu, P.B. Mögensen, Whisper Investigators, WHISPER, a resonance sounder and wave analyser: Performances and perspectives for the Cluster mission. Space Sci. Rev. **79**(1–2), 157–193 (1997)

P.M.E. Décréau, P. Fergeau, V. Krasnosels'kikh, E. Le Guirriec, M. Lévêque, P. Martin, O. Randriamboarison, J.L. Rauch, F.X. Sené, H.C. Séran, J.G. Trotignon, P. Canu, N. Cornilleau, H. de Féraudy, H. Alleyne, K. Yearby, P.B. Mögensen, G. Gustafsson, M. André, D.A. Gurnett, F. Darrouzet, J. Lemaire, C.C. Harvey, P. Travnicek, Whisper experimenters, Early results from the Whisper instrument on Cluster: an overview. Ann. Geophys. **19**(10–12), 1241–1258 (2001)

P.M.E. Décréau, C. Ducoin, G. Le Rouzic, O. Randriamboarison, J.L. Rauch, X. Trotignon, J.G. Vallières, P. Canu, F. Darrouzet, M.P. Gough, A.M. Buckley, T.D. Carozzi, Observation of continuum radiations from the CLUSTER fleet: First results from direction finding. Ann. Geophys. **22**(7), 2607–2624 (2004)

P.M.E. Décréau, E. Le Guirriec, J.L. Rauch, J.G. Trotignon, P. Canu, F. Darrouzet, J. Lemaire, A. Masson, F. Sedgemore, M. André, Density irregularities in the plasmasphere boundary player: Cluster observations in the dusk sector. Adv. Space Res. **36**(10), 1964–1969 (2005)

Z.C. Dent, I.R. Mann, F.W. Menk, J. Goldstein, C.R. Wilford, M.A. Clilverd, L.G. Ozeke, A coordinated ground-based and IMAGE satellite study of quiet-time plasmaspheric density profiles. Geophys. Res. Lett. **30**(12), 1600 (2003)

R.E. Denton, Magneto-seismology using spacecraft observations, in *Magnetospheric ULF Waves: Synthesis and New Directions*, ed. by K. Takahashi, P.J. Chi, R.E. Denton, R.L. Lysak. Geophysical Monograph Series, vol. 169 (American Geophysical Union, Washington, 2006), pp. 307–317

R.E. Denton, P. Décréau, M.J. Engebretson, F. Darrouzet, J.L. Posch, C. Mouikis, L.M. Kistler, C.A. Cattell, K. Takahashi, S. Schäfer, J. Goldstein, Field line distribution of density at $L = 4.8$ inferred from observations by CLUSTER. Ann. Geophys. (2008, submitted)

F. El-Lemdani Mazouz, J.L. Rauch, P.M.E. Décréau, J.G. Trotignon, X. Vallières, F. Darrouzet, P. Canu, X. Suraud, Wave emissions at half electron gyroharmonics in the equatorial plasmasphere region: CLUSTER observations and statistics. Adv. Space Res. (2008, in press)

R.C. Elphic, L.A. Weiss, M.F. Thomsen, D.J. McComas, M.B. Moldwin, Evolution of plasmaspheric ions at geosynchronous orbit during times of high geomagnetic activity. Geophys. Res. Lett. **23**(16), 2189–2192 (1996)

C.P. Escoubet, C.T. Russell, R. Schmidt (eds.), *The Cluster and Phoenix Missions* (Kluwer Academic, Dordrecht, 1997)

J.C. Foster, P.J. Erickson, A.J. Coster, J. Goldstein, F.J. Rich, Ionospheric signatures of plasmaspheric tails. Geophys. Res. Lett. **29**(13), 1623 (2002)

J.C. Foster, A.J. Coster, P.J. Erickson, W. Rideout, F.J. Rich, T.J. Immel, B.R. Sandel, Redistribution of the stormtime ionosphere and the formation of the plasmaspheric bulge, in *Inner Magnetosphere Interactions: New Perspectives from Imaging*, ed. by J.L. Burch, M. Schulz, H. Spence. Geophysical Monograph Series, vol. 159 (American Geophysical Union, Washington, 2005), pp. 277–289

B.J. Fraser, J.L. Horwitz, J.A. Slavin, Z.C. Dent, I.R. Mann, Heavy ion mass loading of the geomagnetic field near the plasmapause and ULF wave implications. Geophys. Res. Lett. **32**, L04102 (2005)

S.F. Fung, R.F. Benson, D.L. Carpenter, B.W. Reinisch, D.L. Gallagher, Investigations of irregularities in remote plasma regions by radio sounding: applications of the radio plasma imager on image. Space Sci. Rev. **91**(1–2), 391–419 (2000)

D.L. Gallagher, M.L. Adrian, Two-dimensional drift velocities from the IMAGE EUV plasmaspheric imager. J. Atmos. Sol.-Terr. Phys. **69**(3), 341–350 (2007)

D.L. Gallagher, P.D. Craven, R.H. Confort, Global core plasma model. J. Geophys. Res. **105**(A8), 18819–18833 (2000)

D.L. Gallagher, M.L. Adrian, M.W. Liemohn, Origin and evolution of deep plasmaspheric notches. J. Geophys. Res. **110**, A09201 (2005)

Y.I. Galperin, V.S. Soloviev, K. Torkar, J.C. Foster, M.V. Veselov, Predicting plasmaspheric radial density profiles. J. Geophys. Res. **102**(A2), 2079–2091 (1997)

D.A. Galvan, M.B. Moldwin, B.R. Sandel, Diurnal variation in plasmaspheric He^+ inferred from extreme ultraviolet images. J. Geophys. Res. **113**, A09216 (2008)

L.N. Garcia, S.F. Fung, J.L. Green, S.A. Boardsen, B.R. Sandel, B.W. Reinisch, Observations of the latitudinal structure of plasmaspheric convection plumes by IMAGE-RPI and EUV. J. Geophys. Res. **108**(A8), 1321 (2003)

J. Goldstein, Plasmasphere response: Tutorial and review of recent imaging results. Space Sci. Rev. **124**(1–4), 203–216 (2006)

J. Goldstein, B.R. Sandel, The global pattern of evolution of plasmaspheric drainage plumes, in *Inner Magnetosphere Interactions: New Perspectives from Imaging*, ed. by J.L. Burch, M. Schulz, H. Spence. Geophysical Monograph Series, vol. 159 (American Geophysical Union, Washington, 2005), pp. 1–22

J. Goldstein, R.W. Spiro, P.H. Reiff, R.A. Wolf, B.R. Sandel, J.W. Freeman, R.L. Lambour, IMF-driven overshielding electric field and the origin of the plasmaspheric shoulder of May 24, 2000. Geophys. Res. Lett. **29**(16), 1819 (2002)

J. Goldstein, B.R. Sandel, W.T. Forrester, P.H. Reiff, IMF-driven plasmasphere erosion of 10 July 2000. Geophys. Res. Lett. **30**(3), 1146 (2003a)

J. Goldstein, M. Spasojević, P.H. Reiff, B.R. Sandel, W.T. Forrester, D.L. Gallagher, B.W. Reinisch, Identifying the plasmapause in IMAGE EUV data using IMAGE RPI in situ steep density gradients. J. Geophys. Res. **108**(A4), 1147 (2003b)

J. Goldstein, B.R. Sandel, M.R. Hairston, S.B. Mende, Plasmapause undulation of 17 April 2002. Geophys. Res. Lett. **31**, L15801 (2004a)

J. Goldstein, B.R. Sandel, M.F. Thomsen, M. Spasojević, P.H. Reiff, Simultaneous remote sensing and in situ observations of plasmaspheric drainage plumes. J. Geophys. Res. **109**, A03202 (2004b)

J. Goldstein, J.L. Burch, B.R. Sandel, S.B. Mende, P.C. Brandt, M.R. Hairston, Coupled response of the inner magnetosphere and ionosphere on 17 April 2002. J. Geophys. Res. **110**, A03205 (2005a)

J. Goldstein, B.R. Sandel, W.T. Forrester, M.F. Thomsen, M.R. Hairston, Global plasmasphere evolution 22-23 April 2001. J. Geophys. Res. **110**, A12218 (2005b)

J. Goldstein, B.R. Sandel, H.U. Frey, S.B. Mende, Multiple plasmapause undulations observed by the IMAGE satellite on 20 March 2001. J. Atmos. Sol.-Terr. Phys. **69**(3), 322–333 (2007)

J.M. Grebowsky, Model study of plasmapause motion. J. Geophys. Res. **75**(22), 4329–4333 (1970)

J.L. Green, S. Boardsen, S.F. Fung, H. Matsumoto, K. Hashimoto, R.R. Anderson, B.R. Sandel, B.W. Reinisch, Association of kilometric continuum radiation with plasmaspheric structures. J. Geophys. Res. **109**, A03203 (2004)

R.S. Grew, F.W. Menk, M.A. Clilverd, B.R. Sandel, Mass and electron densities in the inner magnetosphere during a prolonged disturbed interval. Geophys. Res. Lett. **34**, L02108 (2007)

K.I. Gringauz, V.V. Bezrukikh, V.D. Ozerov, R.E. Rybechinsky, The study of the interplanetary ionized gas, high-energy electrons and corpuscular radiation of the Sun, employing threeelectrode charged particle traps on the second Soviet space rocket. Sov. Phys. Dokl. **5**, 361–364 (1960). Published again in (1962) in Planet. Space Sci., **9**, 103–107

G. Gustafsson, M. André, T. Carozzi, A.I. Eriksson, C.G. Fälthammar, R. Grard, G. Holmgren, J.A. Holtet, N. Ivchenko, T. Karlsson, Y. Khotyaintsev, S. Klimov, H. Laakso, P.A. Lindqvist, B. Lybekk, G. Marklund, F. Mozer, K. Mursula, A. Pedersen, B. Popielawska, S. Savin, K. Stasiewicz, P. Tanskanen, A. Vaivads, J.E. Wahlund, First results of electric field and density observations by Cluster EFW based on initial months of observations. Ann. Geophys. **19**(10–12), 1219–1240 (2001)

A. Hasegawa, Drift-wave instability at the plasmapause. J. Geophys. Res. **76**(22), 5361–5364 (1971)

M. Hayakawa, Association of whistlers with lightning discharges on the Earth and on Jupiter. J. Atmos. Terr. Phys. **57**(5), 525–535 (1995)

R.A. Helliwell, *Whistlers and Associated Ionospheric Phenomena* (Stanford University Press, Stanford, 1965)

T.W. Hill, Inertial limit on corotation. J. Geophys. Res. **84**(A11), 6554–6558 (1979)

J.L. Horwitz, R.H. Comfort, C.R. Chappell, A statistical characterization of plasmasphere density structure and boundary locations. J. Geophys. Res. **95**(A6), 7937–7947 (1990)

M.C. Kelley, *The Earth's Ionosphere: Plasma Physics and Electrodynamics* (Academic Press, San Diego, 1989)

K.H. Kim, J. Goldstein, D. Berube, Plasmaspheric drainage plume observed by the Polar satellite in the prenoon sector and the IMAGE satellite during the magnetic storm of 11 April 2001. J. Geophys. Res. **112**, A06237 (2007)

H.C. Koons, Observations of large-amplitude, Whistler mode wave ducts in the outer plasmasphere. J. Geophys. Res. **94**(A11), 15393–15397 (1989)

J. Krall, J.D. Huba, J.A. Fedder, Simulation of H^+ and He^+ dynamics during plasmasphere refilling. Eos Trans. AGU **88**(52), SM21A–0303 (2007)

R.L. Lambour, L.A. Weiss, R.C. Elphic, M.F. Thomsen, Global modeling of the plasmasphere following storm sudden commencements. J. Geophys. Res. **102**(A11), 24351–24368 (1997)

M.J. LeDocq, D.A. Gurnett, R.R. Anderson, Electron Number Density Fluctuations near the Plasmapause Observed by the CRRES Spacecraft. J. Geophys. Res. **99**(A12), 23661–23671 (1994)

J.F. Lemaire, The "Roche-limit" of ionospheric plasma and the formation of the plasmapause. Planet. Space Sci. **22**(5), 757–766 (1974)

J.F. Lemaire, The mechanisms of formation of the plasmapause. Ann. Geophys. **31**, 175–190 (1975)

J.F. Lemaire, *Frontiers of the Plasmasphere*. Aeronomica Acta, vol. 298. (Editions Cabay, Louvain–la–Neuve, 1985). ISBN 2-87077-310-2
J.F. Lemaire, Plasma distribution models in a rotating magnetic dipole and refilling plasmaspheric flux tubes. Phys. Fluids B **1**(7), 1519–1525 (1989)
J.F. Lemaire, The formation plasmaspheric tails. Phys. Chem. Earth (C) **25**, 9–17 (2000)
J.F. Lemaire, The formation of the light-ion-trough and peeling off the plasmasphere. J. Atmos. Sol.-Terr. Phys. **63**(11), 1285–1291 (2001)
J.F. Lemaire, K.I. Gringauz, *The Earth's Plasmasphere* (Cambridge University Press, New York, 1998)
J.F. Lemaire, R.W. Schunk, Plasmaspheric wind. J. Atmos. Terr. Phys. **54**(3–4), 467–477 (1992)
J.F. Lemaire, R.W. Schunk, Plasmaspheric convection with non-closed streamlines. J. Atmos. Terr. Phys. **56**(12), 1629–1633 (1994)
B.T. Loftus, T.E. Van Zandt, W. Calvert, Observations of conjugate ducting by the fixed-frequency topside-sounder satellite. Ann. Geophys. **22**(4), 530–537 (1966)
A. Masson, O. Santolík, D.L. Carpenter, F. Darrouzet, P.M.E. Décréau, F. El-Lemdani Mazouz, J.L. Green, S. Grimald, F. El-Lemdani Mazouz, M.B. Moldwin, F. Němec, Advances in Plasmaspheric Wave Research with CLUSTER and IMAGE Observations. Space Sci. Rev. (2008). This issue
C.E. McIlwain, Coordinates for Mapping the Distribution of Magnetically Trapped Particles. J. Geophys. Res. **66**(11), 3681–3691 (1961)
E.V. Mishin, W.J. Burke, Stormtime coupling of the ring current, plasmasphere, and topside ionosphere: Electromagnetic and plasma disturbances. J. Geophys. Res. **110**, A07209 (2005)
M.B. Moldwin, M.F. Thomsen, S.J. Bame, D.J. McComas, K.R. Moore, An examination of the structure and dynamics of the outer plasmasphere using multiple geosynchronous satellites. J. Geophys. Res. **99**(A6), 11475–11481 (1994)
M.B. Moldwin, M.F. Thomsen, S.J. Bame, D. McComas, G.D. Reeves, The fine-scale structure of the outer plasmasphere. J. Geophys. Res. **100**(A5), 8021–8029 (1995)
M.B. Moldwin, J. Howard, J. Sanny, J.D. Bocchicchio, H.K. Rassoul, R.R. Anderson, Plasmaspheric plumes: CRRES observations of enhanced density beyond the plasmapause. J. Geophys. Res. **109**, A05202 (2004)
D.B. Muldrew, Radio propagation along magnetic field-aligned sheets of ionization observed by the Alouette topside sounder. J. Geophys. Res. **68**(19), 5355–5370 (1963)
G. Murakami, M. Hirai, I. Yoshikawa, The plasmapause response to the southward turning of the IMF derived from sequential EUV images. J. Geophys. Res. **112**, A06217 (2007)
A. Nishida, Formation of plasmapause, or magnetospheric plasma knee, by the combined action of magnetospheric convection and plasma escape from the tail. J. Geophys. Res. **71**(23), 5669–5679 (1966)
P.A. Nsumei, X. Huang, B.W. Reinisch, P. Song, V.M. Vasyliunas, J.L. Green, S.F. Fung, R.F. Benson, D.L. Gallagher, Electron density distribution over the northern polar region deduced from IMAGE/radio plasma imager sounding. J. Geophys. Res. **108**(A2), 1078 (2003)
P.A. Nsumei, B.W. Reinisch, P. Song, J. Tu, X. Huang, Polar cap electron density distribution from IMAGE radio plasma imager measurements: Empirical model with the effects of solar illumination and geomagnetic activity. J. Geophys. Res. **113**, A01217 (2008)
D.M. Ober, J.L. Horwitz, M.F. Thomsen, R.C. Elphic, D.J. McComas, R.D. Belian, M.B. Moldwin, Premidnight plasmaspheric "plumes". J. Geophys. Res. **102**(A6), 11325–11334 (1997)
C.G. Park, Whistler observations of the interchange of ionization between the ionosphere and the protonosphere. J. Geophys. Res. **75**(22), 4249–4260 (1970)
C.G. Park, D.L. Carpenter, Whistler evidence of large-scale electron-density irregularities in the plasmasphere. J. Geophys. Res. **75**(19), 3825–3836 (1970)
C.G. Park, R.A. Helliwell, The formation by electric fields of field-aligned irregularities in the magnetosphere. Radio Sci. **6**(6), 299–304 (1971)
G. Paschmann, J.M. Quinn, R.B. Torbert, H. Vaith, C.E. McIlwain, G. Haerendel, O.H. Bauer, T. Bauer, W. Baumjohann, W. Fillius, M. Förster, S. Frey, E. Georgescu, S.S. Kerr, C.A. Kletzing, H. Matsui, P. Puhl-Quinn, E.C. Whipple, The electron drift instrument on cluster: Overview of first results. Ann. Geophys. **19**(10–12), 1273–1288 (2001)
V. Pierrard, J. Cabrera, Comparisons between EUV/IMAGE observations and numerical simulations of the plasmapause formation. Ann. Geophys. **23**(7), 2635–2646 (2005)
V. Pierrard, J.F. Lemaire, Development of shoulders and plumes in the frame of the interchange instability mechanism for plasmapause formation. Geophys. Res. Lett. **31**, L05809 (2004)
V. Pierrard, J. Goldstein, N. André, V.K. Jordanova, G.A. Kotova, J.F. Lemaire, M.W. Liemohn, H. Matsui, Physics-based models of the plasmasphere. Space Sci. Rev. (2008, this issue)
I.G. Platt, P.L. Dyson, MF and HF propagation characteristics of ionospheric ducts. J. Atmos. Terr. Phys. **51**, 759–774 (1989)

B.W. Reinisch, D.M. Haines, K. Bibl, G. Cheney, I.A. Galkin, X. Huang, S.H. Myers, G.S. Sales, R.F. Benson, S.F. Fung, J.L. Green, S. Boardsen, W.W.L. Taylor, J.L. Bougeret, R. Manning, N. Meyer-Vernet, M. Moncuquet, D.L. Carpenter, D.L. Gallagher, P. Reiff, The Radio Plasma Imager Investigation on the IMAGE Spacecraft. Space Sci. Rev. **91**(1–2), 319–359 (2000)

B.W. Reinisch, X. Huang, P. Song, G.S. Sales, S.F. Fung, J.L. Green, D.L. Gallagher, V.M. Vasyliunas, Plasma density distribution along the magnetospheric field: RPI observations from IMAGE. Geophys. Res. Lett. **28**(24), 4521–4524 (2001)

B.W. Reinisch, X. Huang, P. Song, J.L. Green, S.F. Fung, V.M. Vasyliunas, D.L. Gallagher, B.R. Sandel, Plasmaspheric mass loss and refilling as a result of a magnetic storm. J. Geophys. Res. **109**, A01202 (2004)

H. Rème, C. Aoustin, J.M. Bosqued, I. Dandouras, B. Lavraud, J.A. Sauvaud, A. Barthe, J. Bouyssou, Th. Camus, O. Coeur-Joly, A. Cros, J. Cuvilo, F. Ducay, Y. Garbarowitz, J.L. Médale, E. Penou, H. Perrier, D. Romefort, J. Rouzaud, C. Vallat, D. Alcaydé, C. Jacquey, C. Mazelle, C. d'Uston, E. Möbius, L.M. Kistler, K. Crocker, M. Granoff, C. Mouikis, M. Popecki, M. Vosbury, B. Klecker, D. Hovestadt, H. Kucharek, E. Kuenneth, G. Paschmann, M. Scholer, N. Sckopke, E. Seidenschwang, C.W. Carlson, D.W. Curtis, C. Ingraham, R.P. Lin, J.P. McFadden, G.K. Parks, T. Phan, V. Formisano, E. Amata, M.B. Bavassano-Cattaneo, P. Baldetti, R. Bruno, G. Chionchio, A. Di Lellis, M.F. Marcucci, G. Pallocchia, A. Korth, P.W. Daly, B. Graeve, H. Rosenbauer, V. Vasyliunas, M. McCarthy, M. Wilber, L. Eliasson, R. Lundin, S. Olsen, E.G. Shelley, S. Fuselier, A.G. Ghielmetti, W. Lennartsson, C.P. Escoubet, H. Balsiger, R. Friedel, J.-B. Cao, R.A. Kovrazhkin, I. Papamastorakis, R. Pellat, J. Scudder, B. Sonnerup, First multi-spacecraft ion measurements in and near the Earth's magnetosphere with the identical Cluster Ion Spectrometry (CIS) experiment. Ann. Geophys. **19**(10–12), 1303–1354 (2001)

M.A. Reynolds, G. Ganguli, Y.-J. Su, M.F. Thomsen, The local-time variation of the quiet plasmasphere: Geosynchronous observations and kinetic theory. Ann. Geophys. **21**(11), 2147–2154 (2003)

A.D. Richmond, Self-induced motions of thermal plasma in the magnetosphere and the stability of the plasmapause. Radio Sci. **8**(11), 1019–1027 (1973)

B.R. Sandel, M.H. Denton, Global view of refilling of the plasmasphere. Geophys. Res. Lett. **34**, L17102 (2007)

B.R. Sandel, A.L. Broadfoot, C.C. Curtis, R.A. King, T.C. Stone, R.H. Hill, J. Chen, O.H.W. Siegmund, R. Raffanti, D.D. Allred, R.S. Turley, D.L. Gallagher, The extreme ultraviolet imager investigation for the IMAGE mission. Space Sci. Rev. **91**(1–2), 197–242 (2000)

B.R. Sandel, R.A. King, W.T. Forrester, D.L. Gallagher, A.L. Broadfoot, C.C. Curtis, Initial results from the IMAGE extreme ultraviolet imager. Geophys. Res. Lett. **28**(8), 1439–1442 (2001)

B.R. Sandel, J. Goldstein, D.L. Gallagher, M. Spasojević, Extreme ultraviolet imager observations of the structure and dynamics of the plasmasphere. Space Sci. Rev. **109**(1–4), 25–46 (2003)

N. Singh, Refilling of a plasmaspheric flux tube: microscopic plasma processes, in *Modeling Magnetospheric Plasma*, ed. by T.E. Moore, J.H. Waite. Geophysical Monograph Series, vol. 44 (American Geophysical Union, Washington, 1988), pp. 87–99

N. Singh, J.L. Horwitz, Plasmaspheric refilling: Recent observations and modelling. J. Geophys. Res. **97**(A2), 1049–1079 (1992)

R.L. Smith, Propagation characteristics of whistlers trapped in field-aligned columns of enhanced ionization. J. Geophys. Res. **66**(11), 3699–3707 (1961)

M. Spasojević, J. Goldstein, D.L. Carpenter, U.S. Inan, B.R. Sandel, M.B. Moldwin, B.W. Reinisch, Global response of the plasmasphere to a geomagnetic disturbance. J. Geophys. Res. **108**(A9), 1340 (2003)

M. Spasojević, H.U. Frey, M.F. Thomsen, S.A. Fuselier, S.P. Gary, B.R. Sandel, U.S. Inan, The link between a detached subauroral proton arc and a plasmaspheric plume. Geophys. Res. Lett. **31**, L04803 (2004)

R.W. Spiro, M. Harel, R.A. Wolf, P.H. Reiff, Quantitative simulation of a magnetospheric substorm. 3. Plasmaspheric electric fields and evolution of the plasmapause. J. Geophys. Res. **86**(A4), 2261–2272 (1981)

L.R.O. Storey, An investigation of whistling atmospherics. Philos. Trans. R. Soc. (Lond.) **246A**, 113–141 (1953)

H.J. Strangeways, M.J. Rycroft, Trapping of whistler-waves through the side of ducts. J. Atmos. Terr. Phys. **42**, 983–994 (1980)

Y. Su, M.F. Thomsen, J.E. Borovsky, J.C. Foster, A linkage between polar patches and plasmaspheric drainage plumes. Geophys. Res. Lett. **28**(1), 111–113 (2001)

D. Summers, B. Ni, N.P. Meredith, R.B. Horne, R.M. Thorne, M.B. Moldwin, R.R. Anderson, Electron scattering by whistler-mode ELF hiss in plasmaspheric plumes, J. Geophys. Res. **113**, A04219 (2008)

G. Tarcsai, Ionosphere-plasmasphere electron fluxes at middle latitudes obtained from whistlers. Adv. Space Res. **5**(4), 155–158 (1985)

H.A. Taylor Jr., J.M. Grebowsky, W.J. Walsh, Structured variations of the plasmapause: Evidence of a corotating plasma tail. J. Geophys. Res. **76**(28), 6806–6814 (1971)

R.J. Thomson, The formation and lifetime of whistler ducts. Planet. Space Sci. **26**(5), 423–430 (1978)

J.G. Trotignon, P.M.E. Décréau, J.L. Rauch, E. Le Guirriec, P. Canu, F. Darrouzet, The whisper relaxation sounder onboard cluster: A powerful tool for space plasma diagnosis around the Earth. Cosm. Res. **41**(4), 369–372 (2003)

N.A. Tsyganenko, D.P. Stern, Modeling the global magnetic field of the large-scale Birkeland current systems. J. Geophys. Res. **101**(A12), 27187–27198 (1996)

J. Tu, P. Song, B.W. Reinisch, X. Huang, J.L. Green, H.U. Frey, P.H. Reiff, Electron density images of the middle- and high-latitude magnetosphere in response to the solar wind. J. Geophys. Res. **110**, A12210 (2005)

J. Tu, P. Song, B.W. Reinisch, J.L. Green, X. Huang, Empirical specification of field-aligned plasma density profiles for plasmasphere refilling. J. Geophys. Res. **111**, A06216 (2006)

J. Tu, P. Song, B.W. Reinisch, J.L. Green, Smooth electron density transition from plasmasphere to the sub-auroral region. J. Geophys. Res. **112**, A05227 (2007)

C.L. Waters, F.W. Menk, M.F. Thomsen, C. Foster, F.R. Fenrich, Remote sensing of the magnetosphere using ground-based observations of ULF waves, in *Magnetospheric ULF Waves: Synthesis and New Directions*, ed. by K. Takahashi, P.J. Chi, R.E. Denton, R.L. Lysak. Geophysical Monograph Series, vol. 169 (American Geophysical Union, Washington, 2006), pp. 319–340

G.R. Wilson, J.L. Horwitz, J. Lin, A semikinetic model for early stage plasmasphere refilling. 1. Effects of coulomb collisions. J. Geophys. Res. **97**(A2), 1109–1119 (1992)

E. Yizengaw, M.B. Moldwin, The altitude extension of the mid-latitude trough and its correlation with plasmapause position. Geophys. Res. Lett. **32**, L09105 (2005)

E. Yizengaw, H. Wei, M.B. Moldwin, D. Galvan, L. Mandrake, A. Mannucci, X. Pi, The correlation between mid-latitude trough and the plasmapause. Geophys. Res. Lett. **32**, L10102 (2005)

E. Yizengaw, M.B. Moldwin, D.A. Galvan, Ionospheric signatures of a plasmaspheric plume over Europe. Geophys. Res. Lett. **33**, L17103 (2006)

E. Yizengaw, J. Dewar, J. MacNeil, M.B. Moldwin, D. Galvan, J. Sanny, D. Berube, B. Sandel, The occurrence of ionospheric signatures of plasmaspheric plumes over different longitudinal sectors. J. Geophys. Res. **113**, A08318 (2008)

I. Yoshikawa, A. Yamazaki, K. Yamashita, Y. Takizawa, M. Nakamura, Which is a significant contributor for outside of the plasmapause, an ionospheric filling or leakage of plasmaspheric materials?: Comparison of He II (304 Å) images. J. Geophys. Res. **108**(A2), 1080 (2003)